Quantum transport in topological insulators

–

superconductor heterostructures

Bachelor thesis
by
Johannes Krotz

elaborated at

HÁSKÓLINN Í REYKJAVÍK
REYKJAVIK UNIVERSITY

and submitted on the

1st Sept. 2015

to

Universität
Konstanz

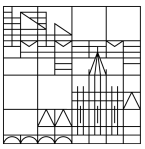

Department of Physics

1. evaluated by Professor Dr. W. Belzig (University of Constance)
2. evaluated by Ass.-Professor Dr. S. I. Erlingsson (Reykjavik University)


I'm afraid we need to use
math.
VIA 9GAG.COM

Abstract:

The edge states of the 2-dimensional time reversal invariant topological insulator HgTe/CdTe in the inverted regime, were reproduced. Such a topological insulator is described by the effective four-band BHZ(Bernevig-Hughes-Zhang)-model, which reveals edge states unaffected by back scattering for certain choices of parameters.
Further the influence of a magnetic barrier and induced superconductivity on the edge states was examined. Namely the effective g-factor $\hat{g}$ and the effective superconducting order parameter α where introduced.
Finally a way is suggested to experimentally gain information about the g-factors g_E and g_H and about the superconducting order parameters Δ_E and Δ_H of the bands of the BHZ-model. g_E and g_H are coupling the four Bands of the BHZ-model in presence of a magnetic field, while Δ_E and Δ_H couple electrons in these bands to their hole-partners, if the topological insulator is in proximity to a superconductor.

Zusammenfassung:

Die Randzustände des 2-dimensionalen zeitumkehr-invarianten topologischen Isolators HgTe/CdTe mit invertierter Bandstruktur wurden reproduziert. Besagter topologischer Isolator wird durch das effektive vier-Band BHZ(Bernevig-Hughes-Zhang)-Model beschrieben, welches topologische Randzustände für bestimmte Parameterwerte zulässt.
Ferner wurde der Einfluss einer magnetischen Bariere sowie induzierte Supraleitfähigkeit auf besagte Randzustände untersucht. Insbesondere wurden der effektive g-Faktor $\hat{g}$ sowie der effektive (Supraleitungs-) Ordnungs-Parameter α eingeführt.
Zu guter Letzt wird ein Vorschlag zur experimentellen Bestimmung der Subband g-Faktoren g_E und g_H sowie der Subband Ordnungs Parameter Δ_E und Δ_H aus den jeweiligen effektiven Größen $\hat{g}$ und α unterbreitet. g_E und g_H vermitteln in Anwesenheit eines magnetischen Feldes eine lineare Kopplung zwischen den 4 Bändern des BHZ-Models, während Δ_E und Δ_H eine Kopplung zwischen Elektronen dieser 4 Bänder und deren Loch-Partner vermitteln, falls sich der topologische Isolator in der Nähe eines Supraleiters befindet.

Contents

Acknowledgements

I would like to express my gratitude to Wolfgang Belzig and Sigurður Erlingson for making my magnificent stay in Iceland possible. In particular I would like to thank Siggi, who had to endure all my more and less stupid questions and my sometimes oh so limited perceptivity. Without his guidance this thesis would have ended 5 pages before this one.
And finally, since I do it so rarely, i would like express my appreciation to new and old friends and my family for always encouraging me in and sometimes effortlessly distracting me from whatever I am doing.

1 Introduction

Topological insulators are a novel state of matter first predicted in 1987 [1] in 2D-quantum wells of HgTe between CdTe and were first experimentally observed in 2007[2]. Since then topological states were predicted and observed in several other materials as well including 3D systems. Here we will focus in 2D-systems.
These so called topologically insulating states are characterized by the existence of symmetry protected conducting and gapless states on its surface , while its interior resembles a classical insulator, i.e. the Fermi level falls between the valence and the conductance band. These gapless states, behaving like massless relativistic particles, underlie spin-momentum locking protected by time reversal symmetry. Next to possible applications in spintronics or quantum computation, the possible occurrence of Majorana quasi-particles on the surface of topological insulators in proximity to a superconductor or topological superconductors has been a driving motor of the studies of topological insulators over the last decade.

This thesis will keep focus on the 2-dimensional topological insulator first predicted and experimentally realized: a HgTe/CdTe quantum well. After a short introduction to topological insulators in general an effective Model describing this set up will be introduced and it will be shown how it leads to the emergence of the helical edge states characteristic for a topological insulator. In the subsequent chapters the influence of the breaking of time reversal symmetry by a magnetic barrier and the effects of different set ups of superconductors in direct proximity to the topological insulator will be discussed. In the final chapter an experimental way will be suggested to determine the subband g-factors and superconducting order parameters of the model.

2 Topological insulators

This section will be devoted to explaining, what topological insulators are. As the name correctly suggest, that they are a kind of band insulator. This general term will be exemplified in the next subsection, while the difference between topological insulators and non-topological, or topologically trivial, insulators will be elaborated subsequently.

2.1 Band insulators

Exploiting the translational symmetry of a crystal the Hamiltonian of the system can be reduced to and solved on one unit cell of the crystal. These solutions are the so-called Bloch states $|u_n(k)\rangle$, depending on the crystal momentum k, which is defined in the Brillouin zone. The associated eigenvalues $E_n(k)$ define the band structure of the system. Due to the fermionic nature of electrons (Pauli principle) all states up to the chemical potential (,Fermi niveau,) are occupied at zero temperature.

Since fully occupied bands do not contribute to charge transport, insulators are characterized by a totally occupied valence band and an empty conductance band, separated by an energy gap E_Δ[3]. The same applies of course for semiconductors, which seem to be indistinguishable from insulators except for the size of E_Δ. In fact it is possible to manipulate the Hamiltonians continuously, turning an insulator's Hamiltonian into a semiconductor's and vice versa, without closing the gap. We call them topologically equivalent.
In a model reducing the band structure to the valence and conducting band only, i.e. ignoring occupied bands below the valence band and empty bands above the conducting band, all customary insulators are topologically equivalent. They are also equivalent to the vacuum, as it is described in Dirac's relativistic quantum theory. With the infinite reservoir of particles with negative energy(Dirac sea), corresponding to the valence band, the energy needed to create an electron and a positron being E_Δ and states with positive energy corresponding to the conductance band(compare figure 2.1)[4].

All insulators and semiconductors equivalent to the vacuum will henceforth be called topologically trivial. (compare: [5],[6])

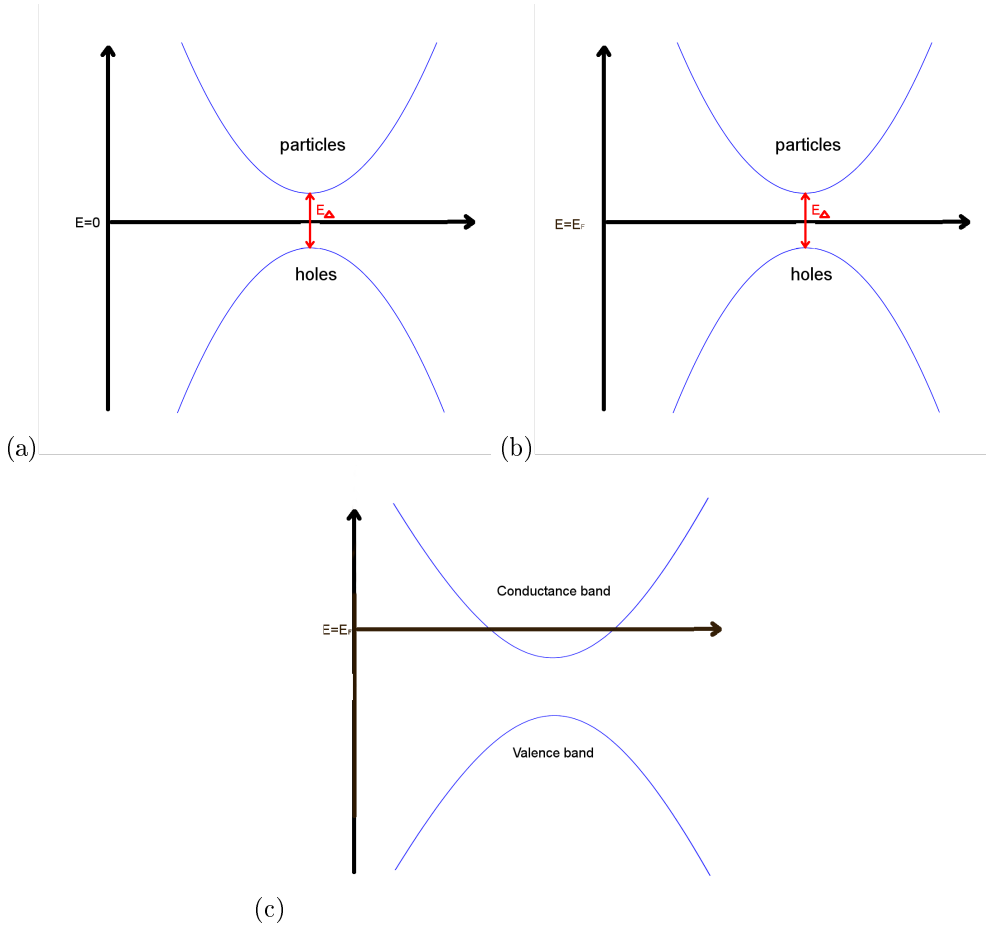

Figure 2.1: Qualitative band structure for the vacuum (a), a semiconductor (b) and a metal (c)

The introduction of the term "topologically trivial" already implies, that there will be topologically non-trivial insulators as well, later simply referred to as "topological insulators". They will be characterized by an insulating bulk and metallic behaviour at the surface. Examples will be given subsequently.

2.2 Quantum Hall effect

The quantum Hall effect is obviously the quantum mechanical analogue to the classical hall effect. It can be observed in two-dimensional electron systems at low temperatures and high magnetic fields. It manifests itself in the quantisation of the hall conductance

$$\sigma = n\frac{e^2}{\hbar} := nG_0; \qquad\qquad n \in \mathbb{N}_0;$$

To understand how this is an example for a topological non trivial state it makes sense to take a look at the Hamiltonian of a electron confined to the x-y-plane in the presence of a magnetic field $\vec{B}$ generated by the vector potential $\vec{A}$.

$$H^B_{x,y} = \frac{1}{2m}\left(\vec{p} + e\vec{A}\right)^2 := \frac{1}{2m}\left(\Pi_x^2 + \Pi_y^2\right), \tag{1}$$

where $\vec{p}$ is the electron's momentum [7]. In the Landau gauge, $\vec{A}_L = -yB\,(1,0,0)$ it is straightforward to show, that $H^B_{x,y}$ can be rewritten as

$$H^B_{x,y} = \hbar\omega_c \left(a^\dagger a + \frac{1}{2}\right), \tag{2}$$

where

$$a = \frac{l_B}{\sqrt{2}\hbar}\,(\Pi_x - i\Pi_y); \qquad\qquad a^\dagger = \frac{l_B}{\sqrt{2}\hbar}\,(\Pi_x + i\Pi_y)$$

are ladder operators with $[a, a^\dagger] = 1$, $l_B = \sqrt{\hbar/eB}$ is the magnetic length and $\omega_c = \hbar/ml_B^2$ the cyclotron frequency. The corresponding energy eigenvalues to $H^B_{x,y}$ and thus the band structure is given by

$$E_m = \hbar\omega_c \left(m + \frac{1}{2}\right); \qquad\qquad m \in \mathbb{N}_0. \tag{3}$$

These energy levels are called Landau-levels. Semi-classically this can be understood as electrons being forced on a circular trajectories with cyclotron frequency ω_c by the magnetic field.
If now m bands are filled with electrons, once again an energy gap separates the occupied bands from the empty bands, like in the case of an insulator. However unlike a conventional insulator the quantum hall system is characterized by the finite Hall-conductivity. This implies that the two systems cannot be equivalent, i.e. their Hamiltonians cannot be continuously turned into each other without closing the gap, which would lead to metallic behaviour.[5][6]

It might seem contradictory, that a system with the bulk band structure of an insulator comes with a finite conductivity. It will turn out that the charge in the quantum Hall system is carried along the edges of the system. Since the quantum Hall system requires a Hall voltage applied to it, it is impossible to create a quantum Hall system without edges. This applied voltage however bends the m occupied Landau-levels on one edge over the Fermi level. Laughlin's gauge argument(compare [7] ch. 6.1) proofs, that a finite current leads to m occupied momenta above the Fermi level at one edge and m empty momenta below the Fermi level at the other edge, manifested m charge carrying states on either edge, each contributing to the conductivity of the edge with G_0. In other words there are m open channels for charge transport on each edge. States on different edges counter propagate. Qualitatively this can be understood in a classical way. In the bulk electrons orbit in circles leading to the Landau levels. At the boundaries however they cannot complete their circular trajectories, but are backscattered instead, which causes them to bounce along the edges(compare figure (2.2)). The counter-propagating, so-called chiral edge states will be characteristic for 2D topological insulators in general.

So far it was discussed, that the vacuum and a quantum Hall system belong to different topological classes. In fact it will turn out, that systems with different Hall conductivity σ belong to different topological classes as well. This seems clear, since the Hall conductivity is related to the number of Landau levels below the Fermi energy. When changing the Hall conductivity of a system from mG_0 to $(m+1)G_0$ by continuously altering the Hamiltonian the gap between the mth and $(m+1)$th Landau level will close and a new one will appear between the $(m+1)$th and the $(m+2)$th, i.e. the topological class changed.
More quantitatively it can be proven, that, if the Hall conductivity σ is the m-fold of the conductivity quantum G_0, then m is the first Chern number of the System.(compare [7] ch. 3)

$$m := \sum_{filledBands} \frac{1}{2\pi} \int_{\mathbb{T}^2} f_n \in \mathbb{Z}, \tag{4}$$

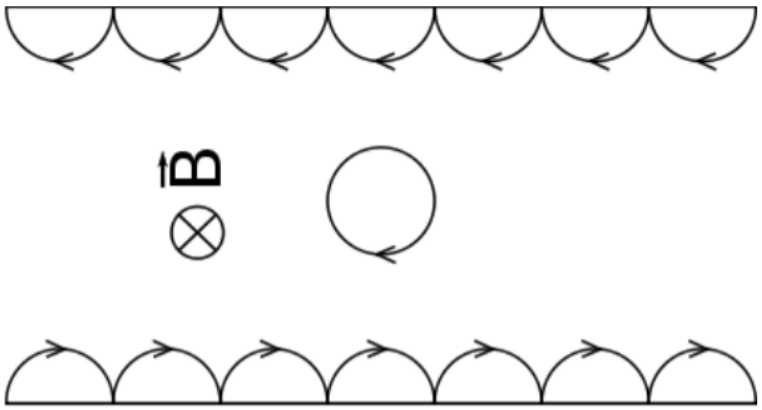

Figure 2.2: Skipping orbit picture or classical explanation for edge current in a quantum hall system

where $f = \frac{\partial}{\partial k_x}\langle u_n(\vec{k})|\frac{-i\partial}{\partial k_y}|u_n(\vec{k}\rangle) - \frac{\partial}{\partial k_y}\langle u_n(\vec{k})|\frac{-i\partial}{\partial k_x}|u_n(\vec{k}\rangle)$ is the Berry curvature, which will be introduced in 2.2, and $\mathbb{T}^2$ is the Brillouin zone, which has due to its periodicity the topological properties of a 2-Torus for a 2-dimensional system. The Chern number gives a distinction between topological classes of vector-bundles, here the Hilbert space vectors, eigenvectors of the Hamiltonian, on a smooth manifold, here the Brillouin zone. Different Chern numbers disprove topological equivalence.[8] The opposite is not the case, nevertheless we will differentiate different topological classes only by their Chern number, i.e. their Hall conductivity in 2D-systems.

Berry phase, Berry connection and Berry curvature

It was stated priorly, that a system's Hall conductance is proportional to the first Chern number, which in turn is the 2πth part of the Berry Phase over a closed path in the Brillouin zone. The terminus Berry-phase will be intruduced in this section.

Consider a general Hamiltonian $H(\vec{\kappa})$ depending on a set of parameters $\vec{\kappa} = (\kappa_1(t), \kappa_2(t), ...)$ with normalized eigenstates $|n(\vec{\kappa})\rangle$ and pairwise different eigenvalues $E_n(\vec{\kappa})$ (For the calculation of the Hall conductance these will be the 2,3-dimensional wave vector $\vec{k}$ and the eigenstates will be the Bloch states.)
The eigenstates of $H(\vec{\kappa})$ will remain eigenstate even if $\vec{\kappa}(t)$ is altered smoothly or in other words moved along a continuous path C in the parameter space. This means though, that an state $|n(\vec{\kappa}(0)\rangle)$ could have only achieved a phase $\vartheta(t)$ during this altering of $\vec{\kappa}(t)$. The time evolution of said state is thereby given by

$$H(\vec{\kappa}(t))e^{-i\vartheta(t)}|n(\vec{\kappa}(t))\rangle = i\hbar\frac{d}{dt}e^{-i\vartheta(t)}|n(\vec{\kappa}(t))\rangle. \tag{5}$$

Multiplication from the left with the bra-state $\langle n(\vec{\kappa}(t))$ leads to a differential equation for the phase $\vartheta(t)$ with solution

$$\vartheta(t) = \frac{1}{\hbar}\int_{t_0}^{t} E_n(\vec{\kappa}(\tau))d\tau - \underbrace{i\int_{t_0}^{t}\langle n(\vec{\kappa}(\tau))|\frac{d}{d\tau}|n(\vec{\kappa}(\tau))\rangle d\tau}_{:=\gamma_n} \tag{6}$$

The first term is the well known energy dependant time evolution, while the second term, defined as γ_n is the Berry-phase.

Further calculation shows, that the Berry phase is in fact time independent.

$$\gamma_n = i\int_{t_0}^{t}\langle n(\vec{\kappa}(\tau))|\frac{\partial}{\partial\vec{\kappa}}|n(\vec{\kappa}(\tau))\rangle\frac{d\vec{\kappa}}{d\tau}d\tau = i\int_C \underbrace{\langle n(\vec{\kappa}(\tau))|\frac{\partial}{\partial\vec{\kappa}}|n(\vec{\kappa}(\tau))\rangle}_{:=A_n(\vec{\kappa})}\,d\vec{\kappa} \tag{7}$$

$A_n(\kappa)$ is called the Berry connection or Berry vector potential. The independence of time combined with the degeneracy of the eigenstate we took for granted, leads to the conclusion that if the path C in the parameter space is a closed loop the phase acquired must be a multiple of 2π, i.e. $\gamma_n = 2\pi m$.

Considering a closed loop and a 3-dimensional parameter space allows to apply Stoke's theorem on the last equation yielding to

$$\gamma_n = i\int d\vec{S}\,(\nabla_{\vec{\kappa}}\times A_n(\vec{\kappa})) = i\int \underbrace{\sum_{i,j,k=1}^{3} dS_i\epsilon_{ijk}\frac{\partial}{\partial\kappa_j}\langle n(\vec{\kappa})|\frac{\partial}{\partial\kappa_k}|n(\vec{\kappa})\rangle}_{:=f_n},$$

where $d\vec{S}$ is the surface of the parameter space and f_n is the Berry curvature. In the special case of $\vec{\kappa} = \vec{k}$ $\partial\vec{S}$ is the Brillouin zone, i.e. a Torus. For a system in the $x-y$-plane, hence $k_z = 0$ and $\frac{\partial}{\partial k_z} = 0$ the Berry curvature has the the same form as stated priorly.[6][7]

3 Time reversal symmetry

Time reversal symmetry is an important concept in the realization of topological insulators, especially concerning the quantum spin Hall insulator, which has zero net Hall conductance, but non vanishing spin transport through the edge channels.

The time reversal operator T reverses the flow of time, i.e.

$$T : t \to -t$$

Signs of operators including odd orders of time explicitly as well as operators including time implicitly, as for example in terms of the time derivative, are changed as well. The other operators remain unchanged. This means, that T will change the sign of the momentum operator $\hat{p}$, while the position operator $\hat{x}$ remains invariant under time reversal. From this a representation of T for spinless particles can be deduced.

$$\begin{aligned} T\,[\hat{x},\hat{p}]\,T^{-1} = -i\hbar = [\hat{x},\hat{p}]^* \\ \Rightarrow T = K, \end{aligned}$$

with K being the operator of complex conjugation.

For spinful particles it has to be considered, that the spin $\hat{S}$, as internal angular momentum, has to be odd under time reversal, i.e. $T\hat{S}T^{-1} = -\hat{S}$, which can be understood as a spin-flip or a rotation by π around any axis in spin space. Therefore one representation can be given as

$$T = e^{-i\pi\hat{S}_y/\hbar}K$$

For spin-$\frac{1}{2}$-particles with $\hat{S} = \frac{\hbar}{2}(\sigma_x,\sigma_y,\sigma_z)$, it leads to

$$T = -i\sigma_y K$$

Note in particular, that $T^2 = -1$. The last fact allows it to proof Kramer's-theorem, which states, that in every time reversal invariant system with an odd number of half-integer spin particles there are two or more degenerate states. [7][12]

Proof. Be $\hat{H}$ the Hamiltonian of a time reversal invariant system, i.e. $\left[\hat{H}, T\right] = 0$, and $|h\rangle$ an already normalized eigenvector to the eigenvalue h.
This implies, that $T|h\rangle$ is an eigenvector to the same eigenvalue.
If $c|h\rangle \neq T|h\rangle$ for $c \in \mathbb{C}$, there are at least two degenerate states as stated by the theorem.

Hence assume: $\exists c \in \mathbb{C}$ with

$$c|h\rangle = T|h\rangle \tag{8}$$

Multiplication with $\langle h|T$ yields using $T^2 = -1$ in

$$-1 = \langle h|T^2|h\rangle = \langle h|Tc|h\rangle = \langle h|c^*T|h\rangle = |c|^2 \not{\downarrow} \tag{9}$$

□

Since they are related via time reversal each per of Kramer-partners have opposite spin.
Kramer's theorem has remarkable consequences for the Hall conductance of time reversal invariant systems. Exploiting, that $T^\dagger = -T$ it can be seen rather quickly, that the berry curvature $f_n(-\vec{k}) = -f_n(\vec{k})$ of the Kramer partners have opposite sign. Since Kramer's theorem states, that these states are degenerate they are either both occupied or both empty, i.e. the Hall conductance is zero.
If the Hall conductivity for each Kramer partner individually is not zero, this leads to an interesting situation called a Quantum spin Hall insulator. State-wise non zero Hall conductivity implies open edge channels for each partner, since due to time reversal symmetry these edge states are counter propagating, this leads evident from the vanishing net Hall conductivity to a zero net charge transport as well. Then again, since the edge states do not only differ in momentum, but also in their spin quantum number, there is a net spin transport along the edges.

4 BHZ-Model

The discussion of the quantum Hall effect as topological property leads to the question, whether topologically non trivial states can only be obtained in presence of a magnetic field. The answer is no, in fact systems described by a simple Dirac Hamiltonian $H_D = \vec{d}\vec{\sigma}$ with $\vec{d} = (k_x, k_y, M)$ exhibit for certain values of M topological edge states carrying charge despite their bulk energy gap.[7]
In this section the existence of edge states will be shown exemplary for a slightly modified Dirac Hamiltonian describing HgTe/CdTe quantum wells, the first topological insulator to be experimentally realized.[2]

These quantum wells consist of a thin layer of HgTe of thickness d between to layers of CdTe. d can be small enough for the whole system to be viewed as 2-dimensional. (In the following a 2 dimensional system in the $x-y-$plane is assumed.Compare 4.1.) The effective in- plane band structure of both materials is described by the subbands E_1, H_1, each double degenerated due to time reversal symmetry. The other bands are far from the other two, why it is neglected, leaving an effective four-band model.Compare figure 4.2

The order of these subbands in HgTe is inverted compared to CdTe. In the quantum well, however, it depends on the thickness of the well, whether the inverted regime is dominant or not. For thickness $d > d_C = 6.3$ nm it is inverted, i.e. $H_1 > E_1$,(Compare fig 5.1.) It turns out that the topologically non trivial state emerges in the inverted structure.

The four-band Hamiltonian will be written in the basis order $|E_1, +\rangle, |H_1, +\rangle, |E_1, -\rangle, |H_1, -\rangle$, where $\pm$ refers to the two Kramer partners on each band. Due to the time reversal invariance of the system the Kramer partners do not couple, hence the off- diagonal 2×2-blocks have to

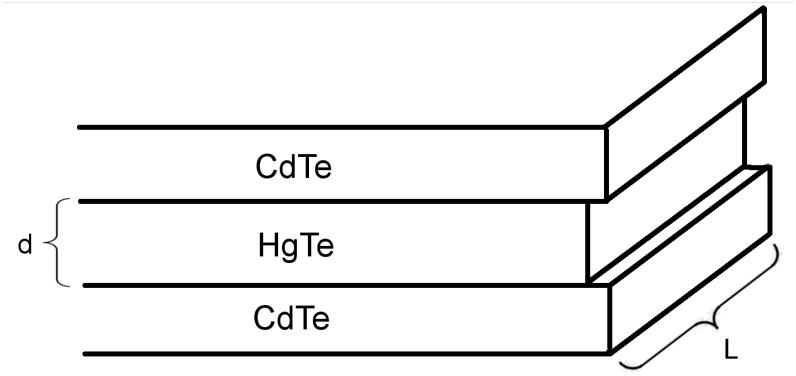

Figure 4.1: schematic of the 2D topological insulator HgTe between layers of CdTe

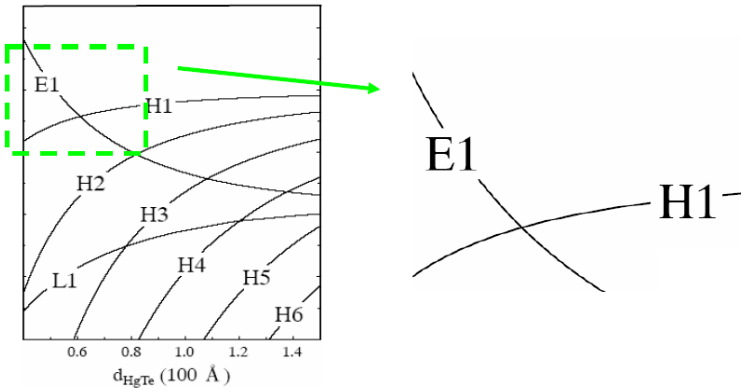

Figure 4.2: Energy of the quantum well in dependency of its thickness d (taken from [P1])

be zero. (The crystal structure of HgTe is not inversion invariant, which would in reality lead to off diagonal bulk inversion asymmetry terms, which however are very small why they will be neglected here, since the do not affect the topological mass term.[9])
The remaining diagonal block will be the time reversed version of the upper one.

E_1- and H_1-bands differ in parity and have a difference of 1 in their orbital quantum number, H_1 is p-like and E_1 is s-like. The the following Hamiltonian, which was first introduced by Bernevig, Hughes and Zhang (BHZ):(compare [10][7][9])

$$\mathcal{H}(\mathbf{k}) = \begin{pmatrix} H(\mathbf{k}) & 0 \\ 0 & H^*(-\mathbf{k}) \end{pmatrix} \tag{10}$$

where

$$H(\mathbf{k}) = \epsilon \mathbf{I}_2 + \vec{d}\vec{s} \tag{11}$$

and

$$\epsilon = C - D(k_x^2 + k_y^2) \tag{12}$$

$$\vec{d} = \begin{pmatrix} Ak_x \\ Ak_y \\ \mathcal{M}(\mathbf{k}) \end{pmatrix} \tag{13}$$

$$\mathcal{M}(\mathbf{k}) = M - B(k_x^2 + k_y^2) \tag{14}$$

$\vec{s} = (s_1, s_2, s_3)$ are the Pauli-Matrices acting on the $E_1 - H_1$-space. The parameters A, B, D, M depend on the geometry (/thickness) of the quantum well. They can be calculated numerically $k \cdot p$-theory.[11]
C is the chemical potential determined by a gate voltage.

4.1 Edge states in BHZ-model

The bulk energy spectrum of this Hamiltonian is

$$E_\pm = C - D(k_x^2 + k_y^2) \pm \sqrt{(M - B(k_x^2 + k_y^2)^2 + A^2(k_x^2 + k_y^2)}, \tag{15}$$

hence it is gapped. This means that the system is an insulator in the bulk. However as we will show edge states can exist. To see if they actually occur in this kind of system the Schrödinger equation has to be solved. Since the Hamiltonian is block diagonal the eigenvalue problem of each block can be solved separately. Conveniently all blocks are related either through time reversal or opposite signs of energy, so that after retrieving the solution for the topmost block the solutions for the other blocks can be derived from it.

For this reason all that remains to solve is the 2-dimensional problem

$$H(\mathbf{k})\Psi = H(\mathbf{k}) \begin{pmatrix} \Psi_1 \\ \Psi_2 \end{pmatrix} = E \begin{pmatrix} \Psi_1 \\ \Psi_2 \end{pmatrix} \tag{16}$$

The chemical potential C is irrelevant for the calculations why it is set to zero for the moment. It can be reintroduced later by the replacement $E \to E - C$.
Assuming an insulator strip with an edge along $y = 0$ and the other one far away at $y = L \to \infty$ and open boundary conditions, i.e. $\Psi(y = 0) = 0 = \Psi(y = L)$, $k_y = p_y/\hbar$ hast to be replaced by the momentum operator $-i\partial_y$. The translation invariance along the x-direction be preserved (periodic boundary conditions), i.e. k_x remains a good quantum number and $\Psi(x) \propto e^{ik_x}$.
Thus the Schrödinger equation becomes the following differential equation:

$$\Leftrightarrow \begin{pmatrix} M - (B + D)(k_x^2 - \partial_y^2) - E & A(k_x - \partial_y) \\ A(k_x + \partial_y) & -M + (B - D)(k_x^2 - \partial_y^2) - E \end{pmatrix} \begin{pmatrix} \Psi_1 \\ \Psi_2 \end{pmatrix} = 0 \tag{17}$$

The Ansatz $\Psi(x, y) = e^{ik_x} e^{\lambda y} \begin{pmatrix} \phi_+ \\ \phi_- \end{pmatrix}$, leads to

$$\begin{pmatrix} M - (B + D)(k_x^2 - \lambda^2) - E & A(k_x - \lambda) \\ A(k_x + \lambda) & -M + (B - D)(k_x^2 - \lambda^2) - E \end{pmatrix} \begin{pmatrix} \phi_1 \\ \phi_2 \end{pmatrix} = 0 \tag{18}$$

If non-zero solutions exist the determinant of this matrix has to be zero.

$$\begin{vmatrix} M - (B + D)(k_x^2 - \lambda^2) - E & A(k_x - \lambda) \\ A(k_x + \lambda) & -M + (B - D)(k_x^2 - \lambda^2) - E \end{vmatrix} = 0 \tag{19}$$

This is a quadratic equation in λ^2, with the following solutions:

$$\lambda_{1,2}^2 = k_x^2 + F \pm \sqrt{F^2 - \frac{(M^2 - E^2)}{B_+ B_-}}. \tag{20}$$

In the last step $F := \frac{A^2 - 2(MB + ED)}{B^2 - D^2}$ was introduced.

Symmetric conduction and valence bands: D=0

To illustrate the procedure the edge states will be calculated for the case $D = 0$, $k_x \approx 0$ and $E \approx 0$. The steps in this special case are very similar to the general case, so that this will help to understand the more complex version as well. [9]

This simplification allows it to display $\lambda_{1,2}$ as

$$\lambda_{1,2}^2 = \frac{1}{4B^2}\left(A \pm \sqrt{A^2 - 4MB}\right)^2 \tag{21}$$

$$\Leftrightarrow \lambda_{1,2} = \pm\frac{1}{2B}\left(A \pm \sqrt{A^2 - 4MB}\right) \tag{22}$$

More interesting than the simplification of $\lambda_{1,2}$ though, is that equation (18) can now be rearranged as follows.

$$(M + B\lambda_{1,2}^2)\underbrace{is_y s_z}_{=s_x}\begin{pmatrix}\phi_1\\ \phi_2\end{pmatrix} = A\lambda_{1,2}\begin{pmatrix}\phi_1\\ \phi_2\end{pmatrix} \tag{23}$$

From which it can be seen that $\begin{pmatrix}\phi_1\\ \phi_2\end{pmatrix}$ has to be an eigenstate of s_x and thus after normalisation either

$$\phi_+ = \tfrac{1}{\sqrt{2}}\begin{pmatrix}1\\ 1\end{pmatrix} \quad \text{or} \quad \phi_- = \tfrac{1}{\sqrt{2}}\begin{pmatrix}1\\ -1\end{pmatrix}.$$

By solving equation (23) as a quadratic equation for $\lambda_{1,2}$ and comparing it to the prior result, it can additionally be seen, that ϕ_+ is the solution for $+\lambda_{1,2}$ and ϕ_- is the solution for $-\lambda_{1,2}$.

Hence there are four linear independent solutions $e^{\pm\lambda_{1,2}}\phi_\pm$ for the Schrödinger equation , i.e. the general solution is a linear combination of them

$$\Psi(x,y) = \left((a_+e^{\lambda_1 y} + b_+e^{\lambda_2 y})\phi_+ + (a_+e^{-\lambda_1 y} + b_+e^{-\lambda_2 y})\phi_-\right)e^{ik_x} \tag{24}$$

The normalizability of $\Psi(x,y)$ implies, that two of the four coefficients have to be zero. The remaining two coefficients can be determined by imposing the boundary conditions $\Psi(x,0) = 0$. It can be differentiated between to cases: either the real parts of λ_1 and λ_2 have the same sign or the opposite sign.
In the second case all four coefficients are zero.This is the topologically trivial state, because no edge states exist. Looking at $\lambda_{1,2}$ one can see that this occurs for $\frac{M}{B} < 0$.
For $\frac{M}{B} > 0$ it turns out, that $a_+ = b_+ = 0$ for $\Re\lambda_{1,2} < 0$ and $a_- = b_- = 0$ for $\Re\lambda_{1,2} > 0$ or else $\Psi(x,y)$ could not be normalized for large L. Furthermore the boundary condition at $y = 0$ requires for the remaining two coefficients $a_\pm = -b_\pm$.

The gathered information leads to the following form of $\Psi(0,y)$:

$$\Psi_{k_x}^\pm(x,y) := e^{ik_x x}\Psi^\pm(0,y) = \frac{a_\pm}{\sqrt{2}}e^{ik_x x}\underbrace{\left(e^{\pm\lambda_1 y} - e^{\pm\lambda_2 y}\right)}_{:=f_\pm(y)}\begin{pmatrix}1\\ \pm 1\end{pmatrix}, \tag{25}$$

where the upper sign belongs to the case $\Re\lambda_{1,2} < 0$, realized for $A/B < 0$ and the lower sign belongs to $\Re\lambda_{1,2} > 0$ for $A/B > 0$.The term $a_\pm$ is a normalisation constant with $\frac{1}{|a_\pm|^2} = \int_0^{L\to\infty}|f_\pm(y)|^2$.

To see, that this state is indeed concentrated on the edge of the insulator strip its absolute square is plotted in figure 4.3 for an exemplary set of A, B, M. It can be seen that the wave function is approximately limited to $0 < y < 200$. The thickness of the quantum well is $d > d_c \approx 61$. Since

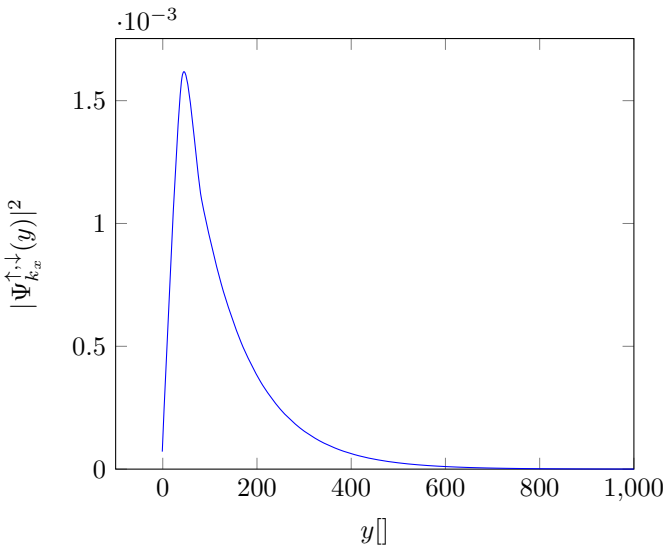

Figure 4.3: probability distribution of edge states for $A = 3.78eV$,$B = -55eV^2$, $M = -0.00015eV$ and quantum well thickness $d = 61.$, compare: [9]

the system is supposed to be 2-dimensional it is safe to assume, that the width L of the strip is much larger than its thickness ($L >> d$) and thus the name edge state is appropriate.
The approximate penetration depth of the general edge states is given by its characteristic length $l_c = |\max\{\lambda_{1,2}\}|^{-1}$. To obtain the dispersion relation of the edge state its energy expectancy value at arbitrary x can be calculated. This corresponds to the projection of topmost block of the bulk Hamiltonian onto its eigenstate.

$$\begin{aligned}\langle\Psi^{\pm}_{k_x}(x,y)|\boldsymbol{H}(\mathbf{k})|\Psi^{\pm}_{k_x}(x,y)\rangle &= \int_0^{L\to\infty}\left(\Psi^{\pm}_{k_x}(x,y)\right)^{\dagger}\boldsymbol{H}(\mathbf{k})\Psi^{\pm}_{k_x}(x,y)dy \\ &= \int_0^{L\to\infty}\frac{1}{2}|a|^2\cdot|f(y)|^2\cdot\begin{pmatrix}1 & \pm1\end{pmatrix}\vec{d_x}\cdot\sigma_x\begin{pmatrix}1\\ \pm1\end{pmatrix}dy = \pm Ak_x\end{aligned} \tag{26}$$

The edge state $\tilde{\Psi}^{\pm}_{k_x}(x,y)$ at $y = L$ will have the form.

$$\tilde{\Psi}^{\pm}_{k_x}(x,y) = \Psi^{\mp}_{k_x}(x,y+L) \tag{27}$$

The change from $\pm$ to $\mp$ is due to the fact that, seen from the right edge, opposite signs of $\lambda_{1,2}$ render normalization impossible. Note, that this is still only true for large L ($L >> d_c$).
Comparing the wave functions at both edges of the strip, it can be seen, that they are basically each other mirror image, mirrored ate the middle of the strip ($y = L/2$), as illustrated in figure 4.4.
Concerning the dispersion relation $\pm$ turn into $\mp$ as well of course. This however has the consequence, that for a fixed energy E the edge states in each edge have to have opposite momentum k_x, i.e. they counter propagate. This can be made clear easily by imagining the tow edges being connected at $x = \infty$ as illustrated in figure 4.5.
Since the states on the right edge do not offer new information from now on the focus will be set solely on the left edge, if not stated differently. Furthermore to increase the clarity it will be assumed that $A/B < 0$, i.e. the lower sign in all equations in this sections will be dropped and the simplified notation $\Psi_{k_x}(x,y) = \Psi^{+}_{k_x}(x,y)$ will be used.

So far only the edge state $\Psi_{k_x}(x,y)$ for the topmost block of the bulk Hamiltonian were calculated.

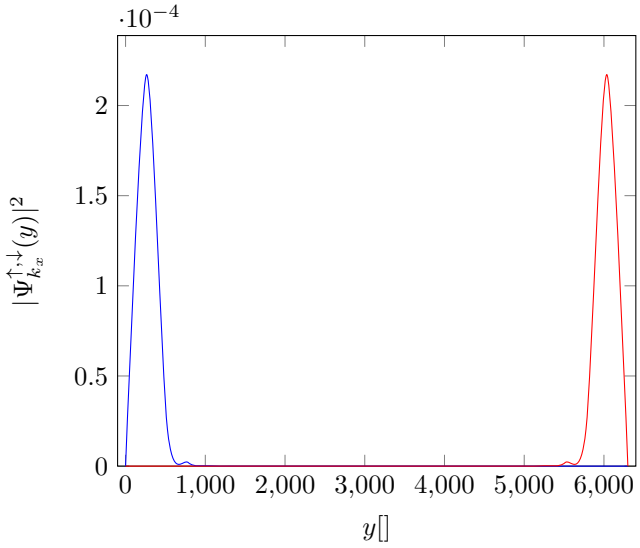

Figure 4.4: probability distribution of $\left|\Psi^{\uparrow}_{k_x}(y)\right|^2$(blue) and $\left|\Psi^{\downarrow}_{k_x}(y)\right|^2$ (red) at different edges. (L=63nm,$A = 3.78eV$,$B = -55eV^2$, $M = -0.00015eV$,$d = 61$

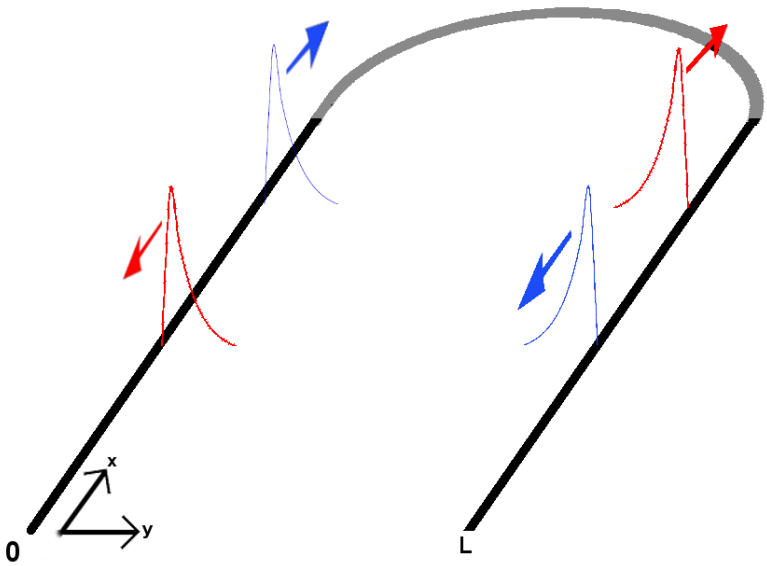

Figure 4.5: qualitative image of counter propagating Kramer partners(red/blue) on each edge and connection of edges at ∞(grey)

However as mentioned previously the solutions for the remaining block can also be deduced from this solution. Since it is the time (and spin) reversed partner of $\Psi_{k_x}(x, y)$ it can be obtained by setting $k_x \to -k_x$.

These considerations lead to the two edge state solution of the Hamiltonian:

$$|1, D=0\rangle = \begin{pmatrix} \Psi_{k_x}(x,y) \\ \vec{0} \end{pmatrix}; \qquad |2, D=0\rangle = \begin{pmatrix} \vec{0} \\ \Psi_{-k_x,}(x,y) \end{pmatrix}$$

where $\pm$ is for counter propagating Kramer partners and e/h refers to electron/hole-like states. Their dispersion relation can be summarized in the effective Hamiltonian (, projection of the Hamiltonian onto the edge states),

$$H^{eff} = A\sigma_z\tau_z, \tag{28}$$

or equivalently

$$H^{eff}_{i,j} = \langle i|\mathcal{H}(\mathbf{k})|j\rangle, \qquad i,j \in \{1,2,3,4\}, \tag{29}$$

where $\langle\cdot|\cdot\rangle = \int_0^{L\to\infty}(\cdot)^\dagger(\cdot)dy$.

Asymmetric conductance and valence bands: D $\neq$ 0

The results for the general BHZ-model $D \neq 0$ can be obtained similarly as in the simplified case. While the general form of $\lambda_{1,2}$ is already known (compare equation (20)), the eigenvectors of the Hamiltonian become unlikely more complicated.

To find them the ansatz $\Psi(x,y) = \frac{1}{\sqrt{1+|w_\pm^{1,2}|^2}} e^{ik_x} e^{\pm\lambda_{1,2}} \begin{pmatrix} 1 \\ w_\pm^{1,2} \end{pmatrix}$ is used.

Plugging this ansatz into the Schrödinger equation again allows it to solve for $w_\pm^{1,2}$ and thus determine the eigenvectors.

$$w_\pm^{1,2} = \frac{A(k_x \pm \lambda_{1,2})}{E + M + (B-D)(\lambda_{1,2}^2 - k_x^2)} \tag{30}$$

So again four linearly independent solutions were found and a general solution can be constructed as a linear combination of them.

$$\Psi(0,y) = a_+^1 e^{\lambda_1 y}\begin{pmatrix} 1 \\ w_+^1 \end{pmatrix} + a_+^2 e^{\lambda_2 y}\begin{pmatrix} 1 \\ w_+^2 \end{pmatrix} + a_-^1 e^{-\lambda_1 y}\begin{pmatrix} 1 \\ w_-^1 \end{pmatrix} + a_-^2 e^{-\lambda_2 y}\begin{pmatrix} 1 \\ w_-^2 \end{pmatrix} \tag{31}$$

Normalizability of $\Psi(x,y)$ requires that all positive exponents vanish. Since the real parts of λ_1 and λ_2 have the same sign this means that either $a_+^1 = a_+^2 = 0$ or $a_-^1 = r_- = 0$. This can also be seen by simply applying the boundary condition $\Psi(x,y)$. Any other combination of vanishing coefficients would require the remaining two coefficients to be zero as well.

This results in

$$\Psi^\pm(0,y) = a_\pm^1 e^{\lambda_1 y}\begin{pmatrix} 1 \\ w_\pm^1 \end{pmatrix} + a_+^2 e^{\lambda_2 y}\begin{pmatrix} 1 \\ w_\pm^2 \end{pmatrix}, \tag{32}$$

where the upper sign as before corresponds to $\Re\lambda_{1,2} < 0$ and vice versa.

To fulfil the boundary condition $\Psi^\pm(0,0) = 0$ the first component of equation (32) requires $a_\pm^1 = -a_\pm^2$. Inserting this into the second component a then leads to $w_\pm := w_\pm^1 = w_\pm^2$. This is a closed equation for the energy E, allowing it to calculate the dispersion relation of the edge states. At the same time the wave function is completely determined.

$$\Psi_{k_x}^\pm(x,y) = \frac{1}{\sqrt{1+|w_\pm(k_x)|^2}} e^{ik_x x} f_\pm(y) \begin{pmatrix} 1 \\ w_\pm(k_x). \end{pmatrix} \tag{33}$$

$$E_\pm = -\frac{DM}{B} \pm A\sqrt{\frac{B^2-D^2}{B^2}}k_x + C \tag{34}$$

Compare[13].
For a better overview the lower sign is dropped in the notation (if the parameters require - instead of + as a solution this can be reintroduced by changing the sign of v_g). If the chemical potential is placed in the middle of the gap, i.e. $C = DM/B$ the dispersion is

$$E = A\sqrt{\frac{B^2 - D^2}{B^2}}k_x := \hbar v_g k_x, \tag{35}$$

with the velocity of the edge states $v_g = A\sqrt{\frac{B^2-D^2}{B^2\hbar^2}}$. As before the edge states for the remaining three blocks and easily be deducted from $\Psi_{k_x}(x, y)$. As a reminder, the two edge states are the following:

$$|1\rangle = \begin{pmatrix} \Psi_{k_x}(x,y) \\ \vec{0} \end{pmatrix}; \qquad |2\rangle = \begin{pmatrix} \vec{0} \\ \Psi_{-k_x,}(x,y) \end{pmatrix} \tag{36}$$

And the effective Hamiltonian of these four states is given by

$$H^{eff} = \hbar v_g \sigma_z. \tag{37}$$

As before the effective Hamiltonian is obtained by projecting the original 4×4 Hamiltonian onto the edge states, or in other words

$$H^{eff}_{i,j} = \langle i|H(k)|j\rangle, \tag{38}$$

with

$$\langle \cdot|\cdot\rangle = \int_0^L (\cdot)^\dagger (\cdot)\, dy. \tag{39}$$

In this reduced Hilbert space the edge states $|1\rangle$ and $|2\rangle$ work as a basis. Note that in the process of projecting the Hamiltonian onto the edge states, which are a superposition of conductance- and valence band states, the information about these two bands was lost. Hence the Hamiltonian contains no more trace of the $\vec{s}$-Pauli matrices, but only of the σ_i acting on the Kramer-spin space. Note that the form of $|\Psi^e_{\pm k_x}|^2$ in y-direction is if $\lambda_{1,2} \in \mathbb{R}$ is qualitatively the same as in the case of $D = 0$. For $\lambda \in \mathbb{C} \setminus i\mathbb{R}$ $\Psi^{e/h}_{\pm k_x}$ will show the behaviour of a periodic function enveloped by a function decaying in y-direction as in the $D = 0$-case. Hence both alternatives lead to states concentrated on the edge. The condition for $\lambda_{1,2} \notin i\mathbb{R}$ are $\frac{A}{B^2-D^2} > 4\frac{M}{B} > 0$ [14]

5 Breaking of time reversal symmetry

So far the effective 2×2 Hamiltonian of the edge states in a system invariant under time reversal was determined. In this section the consequences of a time reversal breaking barrier over the full y-range of the topological insulator will be discussed.In x-direction it shall be situated between $x = 0$ and $x = d_B$ Experimentally this could be realized by putting a ferromagnet on top of the topological insulator device as it can be seen in figure 5.1.

To theoretically realize the breaking of time reversal symmetry the effective Hamiltonian of the edge states has to be modified. A general modification has the following form.

$$H_{mod} = H^{eff} + n_0\sigma_0 + \vec{n}\vec{\sigma} \tag{40}$$

The n_i could be depending on x, it shall be assumed here though that they are constant for $0 < x < d_B$ and zero everywhere else.

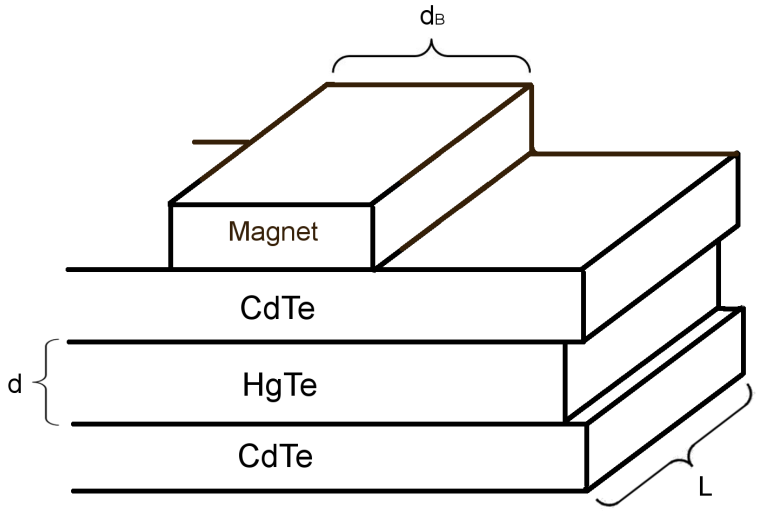

Figure 5.1: schematic of the edge a 2D topological insulator with magnetic barrier

So the effective Hamiltonian along the x-direction for the topological insulator with a magnetic barrier considered here will have the form

$$H^{eff} = \begin{cases} \hbar v_G k_x \sigma_z & \text{for } x < 0 \\ \hbar v_G k_x \sigma_z + C' + \mu_B g \vec{n}\vec{\sigma} & \text{for } 0 < x < d_B \\ \hbar v_G k_x \sigma_z & \text{for } d_B < x \end{cases} \tag{41}$$

Where C' could be a varying chemical potential within the barrier.
In the basis order $|1\rangle, |2\rangle$, the Hamiltonian within the barrier is represented by

$$H^{eff} = \begin{pmatrix} \hbar v_g k_x + C' + n_z & n_x - i n_y \\ n_x + i n_y & -\hbar v_g k_x + C' - n_z \end{pmatrix} \tag{42}$$

The solutions outside of the barrier are obviously the two basis vectors, so that it will be enough to solve the Schrödinger equation within the barrier and then joint the functions continuously.

Note, that within the barrier the energy dispersion of the edge states becomes

$$E = C' \pm \sqrt{\hbar^2 v_g^2 k_x^2 + n_x^2 + n_y^2 + n_z^2}, \tag{43}$$

hence a gap opens in the spectrum, as it can be seen in figure 5.2

Reflectionless propagation:$n_x = n_y = 0$

To show some interesting consequences of intact time reversal symmetry the case $n_x = n_y = 0$, which does not break it will be discussed before the more general case.
To solve the Schrödinger equation within the barrier k_x is replaced by its operator representation $-i\partial_x$, making the equation a first order differential equation. For the upper block it reads as follows.

$$\frac{\hbar v_g}{i} \frac{\partial}{\partial x} \sigma_z \Phi(x) = \left((E - n_0)\mathbb{1} - n_z \sigma_z \right) \Phi(x), \tag{44}$$

which is solved by

$$\Phi(x) = a \cdot e^{i k_x' x} |1\rangle + b \cdot e^{i k_x'' x} |2\rangle, \tag{45}$$

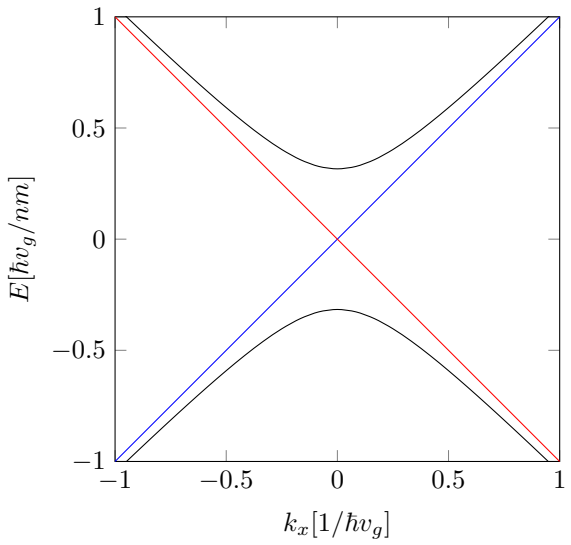

Figure 5.2: energy spectrum of the edge states outside of the barrier (red and blue), inside the barrier (black) for $n_x^2 + n_y^2 + n_z^2 = 0.1\hbar^2 v_g^2/nm^2$, C'=0

where k_x' and k_x'' are defined by

$$k_x' := \frac{E - C' - n_z}{\hbar v_g}; \qquad k_x'' := \frac{E - C' + n_z}{\hbar v_g}.$$

Viewing this as a tunnelling problem a state $|1\rangle$ incoming from the left ($x < 0$) is either reflected back to $x < 0$ into left moving state $|2\rangle$ or transmitted past the barrier into a right moving state $|1\rangle$. Keep in mind, that the states $|1\rangle$ and $|2\rangle$ are counter propagating and hence neither reflection from $|1\rangle$ to $|1\rangle$ nor transmission from $|1\rangle$ to $|2\rangle$ is possible. Assuming no state $|2\rangle$ propagating from the right $x > d_B$ towards the barrier the following boundary conditions for $\Phi(x)$ are obtained:

$$\Phi(0) = |1\rangle + r|2\rangle; \qquad \Phi(d_B) = t|1\rangle,$$

where t and r are transmission respectively reflection amplitudes. Note, that since the Schrödinger equation is a first order differential equation only the functions itself, but none of their derivatives have to be matched at $x = 0$ and $x = d_B$.[4]

Applying these boundary conditions the variables $a = 1$, $b = r = 0$ and $t = e^{ik_x' d_B}$ can be determined. Note that the transmission $T = |t|^2 = 1$ and the reflection $R = |r|^2 = 0$ are absolutely independent of E, C and n_z. It can hereby seen, that intact time reversal symmetry renders all backscattering impossible. The transmission T and reflection R for the states $|2 - 4\rangle$ are the same. The exact form of their transmission and reflection amplitude will be discussed with more generality in the next section.

Qualitatively this can also be understood as an interference effect. When a for example spin-up electron is backscattered into a spin down state the spin has to be rotated by π or $-\pi$. Since the resulting state is a superposition of both possibilities and for spin-1/2-particles a spin difference of 2π corresponds to a factorial difference of -1 the interference is destructive.[6]

Imperfect transmission: $n_x \neq 0 \neq n_y$

Now an arbitrary breaking of time reversal symmetry , i.e. $n_x \neq 0 \neq n_y$(still assuming, that they are constant over $0 < x < d_B$ tough) shall be allowed. This will result into non zero reflection R .

Since the Hamiltonian remains block diagonal the Schrödinger equation can be solved blockwise again. The equation for the upper block is reduced to the following.

$$\frac{\partial}{\partial x}\Phi^* = \frac{i}{\hbar v_g}\left(E\sigma_z - n_z\mathbb{1} + in_x\sigma_y - in_y\sigma_x\right)\Phi^*(x) \tag{46}$$

$$= \underbrace{\frac{1}{\hbar v_g}\begin{pmatrix} i(E-n_0-n_z) & n_y+in_x \\ n_y-in_x & i(-E-n_z)\end{pmatrix}}_{:=M}\Phi^*(x), \tag{47}$$

where $\Phi^* = \sigma_z\Phi$ was introduced. A general solutions to equation (46) is given by

$$\Phi^*(x) = e^{Mx}\left(a|1\rangle - b|2\rangle\right). \tag{48}$$

From this the actual solution $\Phi(x)$ can be derived.

$$\begin{aligned}\Phi(x) =&\sigma_z\Phi^*(x) = \sigma_z e^{Mx}\left(a|1\rangle - b|2\rangle\right)\\ =&e^{\sigma_z M\sigma_z x}\sigma_z\left(a|1\rangle - b|2\rangle\right) = e^{\sigma_z M\sigma_z x}\left(a|1\rangle + b|2\rangle\right)\end{aligned} \tag{49}$$

M is diagonalizable and therefore the matrix exponential $e^{\sigma_z M\sigma_z x}$ can be calculated easily with the result

$$e^{\sigma_z M\sigma_z x} = e^{-i\frac{n_z}{\hbar v_g}x}\begin{pmatrix}\cosh\left(\frac{\nu}{\hbar v_g}x\right) + \frac{iE}{\nu}\sinh\left(\frac{\nu}{\hbar v_g}x\right) & -\frac{(n_y+in_x)\sinh\left(\frac{\nu}{\hbar v_g}x\right)}{\nu}\\ -\frac{(n_y-in_x)\sinh\left(\frac{\nu}{\hbar v_g}x\right)}{\nu} & \cosh\left(\frac{\nu}{\hbar v_g}x\right) - \frac{iE}{\nu}\sinh\left(\frac{\nu}{\hbar v_g}x\right)\end{pmatrix}, \tag{50}$$

and

$$e^{-\sigma_z M\sigma_z x} = e^{i\frac{n_z}{\hbar v_g}x}\begin{pmatrix}\cosh\left(\frac{\nu}{\hbar v_g}x\right) + \frac{-iE}{\nu}\sinh\left(\frac{\nu}{\hbar v_g}x\right) & \frac{(n_y+in_x)\sinh\left(\frac{\nu}{\hbar v_g}x\right)}{\nu}\\ \frac{(n_y-in_x)\sinh\left(\frac{\nu}{\hbar v_g}x\right)}{\nu} & \cosh\left(\frac{\nu}{\hbar v_g}x\right) - \frac{-iE}{\nu}\sinh\left(\frac{\nu}{\hbar v_g}x\right)\end{pmatrix}. \tag{51}$$

In the last step

$$\nu := \sqrt{n_x^2 + n_y^2 - (E)^2} \tag{52}$$

was introduced.
With this collected information the $\Phi(x)$ can be determined for arbitrary boundary conditions and thereby the transmission and reflection amplitudes can be calculated.
Since $|1\rangle$ and $|2\rangle$ are Kramer partners they are always counter propagating. For a given energy $E > 0$ $|1\rangle$ is propagating with positive k_x and $|2\rangle$ with a negative k_x. Hence a the right propagating state $|1\rangle$ will be reflected into the state $|2\rangle$ at the barrier or be transmitted. Same applies for the a state $|2\rangle$ approaching the barrier from the right side. Note, that, if the sign of the energy changes, the sign of k_x changes as well and hence the propagation direction is inverted. From these considerations the boundary conditions shown in table 1 and can be derived. Inserting the

	direction of propagation	bc at x=0	bc at x=d_B
$E > 0$	left $\rightarrow$ right	$\Phi(0) = \|1\rangle + r^e_{\rightarrow}\|2\rangle$	$\Phi(d_B) = t^e_{\rightarrow}\|1\rangle$
$E > 0$	right $\rightarrow$ left	$\Phi(0) = t^e_{\leftarrow}\|2\rangle$	$\Phi(d_B) = \|2\rangle + r^e_{\leftarrow}\|1\rangle$
$E < 0$	right $\rightarrow$ left	$\Phi(0) = t^h_{\leftarrow}\|3\rangle$	$\Phi(d_B) = \|3\rangle + r^h_{\leftarrow}\|4\rangle$
$E < 0$	left $\rightarrow$ right	$\Phi(0) = \|4\rangle + r^h_{\rightarrow}\|3\rangle$	$\Phi(d_B) = t^h_{\rightarrow}\|4\rangle$

Table 1: boundary conditions to determine transmission and reflection amplitudes of the edge states

boundary conditions displayed in table 1 gives linear systems of equations for all transmission and reflection amplitudes. The results obtained are:

$$\begin{aligned} r^e_{\rightarrow} &= \frac{n_y - i n_x}{\nu \coth\left(\frac{\nu}{\hbar v_g} d_B\right) - iE} & r^h_{\rightarrow} &= \frac{n_y + i n_x}{\nu \coth\left(\frac{\nu}{\hbar v_g} d_B\right) - iE} \\ r^e_{\leftarrow} &= \frac{-n_y - i n_x}{\nu \coth\left(\frac{\nu}{\hbar v_g} d_B\right) - iE} & r^h_{\leftarrow} &= \frac{-n_y + i n_x}{\nu \coth\left(\frac{\nu}{\hbar v_g} d_B\right) - iE} \\ t^e_{\rightarrow} &= \tau e^{-i\frac{n_z}{\hbar v_g} x} & t^h_{\rightarrow} &= \tau^* e^{-i\frac{n_z}{\hbar v_g} x} \\ t^e_{\leftarrow} &= \left(t^e_{\rightarrow}\right)^* & t^h_{\leftarrow} &= \left(t^h_{\rightarrow}\right)^* \end{aligned} \tag{53}$$

where τ was defined as

$$\tau := \cosh\left(\frac{\nu}{\hbar v_g} d_B\right) + \frac{iE \sinh\left(\frac{\nu}{\hbar v_g} d_B\right)}{\nu} - \frac{(n_y^2 + n_x^2)\sinh\left(\frac{\nu}{\hbar v_g} d_B\right)}{\nu^2 \coth\left(\frac{\nu}{\hbar v_g} d_B\right) - iE\nu}.$$

If the time reversal symmetry is broken by a magnetic $\vec{B}$ field as proposed in the introduction of this section a spin coupling between the two degenerated conductance band states and between the two valence band states of the form $\mu_B g_{E/H} \vec{\sigma} \vec{B}$ has to be added to the original BHZ-Hamiltonian. The term μ_B is the Bohr magneton and $g_{E/H}$ are the g-factors of the conductance and the valence band.

In the basis order $|E+\rangle$,$|H+\rangle$,$|E-\rangle$, $|H-\rangle$ this additional term to the Hamiltonian has the form

$$H_{Mag} = \begin{pmatrix} \mu_B g_E B_z & 0 & \mu_B g_E (B_x - iB_y) & 0 \\ 0 & \mu_B g_H B_z & 0 & \mu_B g_H (B_x - iB_y) \\ \mu_B g_E (B_x + iB_y) & 0 & -\mu_B g_E B_z & 0 \\ 0 & \mu_B g_H (B_x + iB_y) & 0 & -\mu_B g_H B_z \end{pmatrix}, \tag{54}$$

or shorter

$$H_{Mag} = \mu_B (g_+ + g_- s_z) \vec{\sigma} \vec{B}. \tag{55}$$

where as before $\vec{s}$ are the Pauli matrices acting on the conductance band- valence band space and $\vec{\sigma}$ act on the Kramer-spin space. Further $g_+ = \frac{1}{2}(g_E + g_H)$ and $g_- = \frac{1}{2}(g_E - g_H)$ were introduced.

This Hamiltonian will be, as the BHZ-Hamiltonian before, projected onto the edge states $|1\rangle$ and $|2\rangle$. In this basis it has the form

$$\begin{aligned} H^{eff}_{Mag} =& \mu_B \begin{pmatrix} (g_+ + \hat{\gamma}(k_x) g_-) B_z & (g_+ + \gamma(k_x) g_-)(B_x - iB_y) \\ (g_+ + \gamma(k_x) g_-)(B_x + iB_y) & -(g_+ + \hat{\gamma}(-k_x) g_-) B_z \end{pmatrix} \\ =& \mu_B \left((g_+ + \gamma(k_x) g_-)(\sigma_x B_x + \sigma_y B_y) + \left(g_+ + \frac{g_-}{2}(\hat{\gamma}(k_x) + \hat{\gamma}(-k_x))\right)\sigma_z B_z + \frac{g_-}{2}(\hat{\gamma}(k_x) - \hat{\gamma}(-k_x)) B_z \right). \end{aligned} \tag{56}$$

Here the two terms $\gamma(k_x)$ and $\hat{\gamma}(k_x)$ were introduced. They are defined as

$$\hat{\gamma}(k_x) = \frac{1 - |w(k_x)|^2}{1 + |w(k_x)|^2} \tag{57}$$

and

$$\gamma(k_x) = \frac{1 - w^*(k_x) w(-k_x)}{\sqrt{1 + |w(k_x)|^2}\sqrt{1 + |w(-k_X)|^2}}. \tag{58}$$

Comparing the equation 42 to equation 56 yields to the following relations:

$$n_x = \mu_B \left(g_+ + \gamma(k_x) g_-\right) B_x := \mu_B \hat{g} B_x \tag{59}$$

$$n_y = \mu_B \left(g_+ + \gamma(k_x) g_-\right) B_y := \mu_B \hat{g} B_y \tag{60}$$

$$n_z = \mu_B \left(g_+ \frac{g_-}{2} \left(\hat{\gamma}\left(k_x\right) + \hat{\gamma}\left(-k_x\right)\right)\right) B_z := \mu_B g_z B_z. \tag{61}$$

$\hat{g}$ will be referred to as the effective g-factor from here. The remaining term $\frac{g_-}{2}\left(\hat{\gamma}(k_x) - \gamma(\hat{-k_x})\right) B_z$ acts like a chemical potential, but vanishes for $k_x \approx 0$. Since this limit will be sufficient for all further purposes this term will be ignored from here on.

The remaining terms lead to the following reflection and transmission amplitudes.

$$\begin{aligned}
r^e_{\rightarrow} &= \frac{\mu_B \hat{g}\left(B_y - iB_x\right)}{\nu \coth\left(\frac{\nu}{\hbar v_g} d_B\right) - iE} & r^h_{\rightarrow} &= \frac{\mu_B \hat{g}\left(B_y + iB_x\right)}{\nu \coth\left(\frac{\nu}{\hbar v_g} d_B\right) - iE} \\
r^e_{\leftarrow} &= \frac{\mu_B \hat{g}\left(-B_y - iB_x\right)}{\nu \coth\left(\frac{\nu}{\hbar v_g} d_B\right) - iE} & r^h_{\leftarrow} &= \frac{\mu_B \hat{g}\left(-B_y + iB_x\right)}{\nu \coth\left(\frac{\nu}{\hbar v_g} d_B\right) - iE} \\
t^e_{\rightarrow} &= \tau e^{-i\frac{\mu_B \hat{g}_z B_z}{\hbar v_g} x} & t^h_{\rightarrow} &= \tau^* e^{-i\frac{\mu_B \hat{g}_z B_z}{\hbar v_g} x} \\
t^e_{\leftarrow} &= \left(t^e_{\rightarrow}\right)^* & t^h_{\leftarrow} &= \left(t^h_{\rightarrow}\right)^*
\end{aligned} \tag{62}$$

$$\tau := \cosh\left(\frac{\nu}{\hbar v_g} d_B\right) + \frac{iE \sinh\left(\frac{\nu}{\hbar v_g} d_B\right)}{\nu} - \frac{\left(\mu_B \hat{g}\left(B_y^2 + B_x^2\right)\right) \sinh\left(\frac{\nu}{\hbar v_g} d_B\right)}{\nu^2 \coth\left(\frac{\nu}{\hbar v_g} d_B\right) - iE\nu}$$

with

$$\nu = \sqrt{\mu_B^2 \hat{g}^2 \left(B_x^2 + B_y^2\right) - E^2}. \tag{63}$$

Note, that only the in-plane components B_x and B_y actually change the amplitude of the transmitted state, while B_z only adds a phase. Note further, that reflection $R = |r^{e/h}_{\leftrightarrow}|^2$ and transmission $T = |t^{e/h}_{\leftrightarrow}|^2$ is the same for all states, namely

$$R = \frac{\mu_B^2 \hat{g}^2 \left(B_x^2 + B_y^2\right)}{|\nu|^2 \coth^2\left(\frac{\nu}{\hbar v_g} d_B\right) + E^2} \tag{64}$$

$$T = 1 - R = \left(\cosh^2\left(\frac{\nu}{\hbar v_g} d_B\right) + \frac{E^2}{|\nu|^2} \sinh^2\left(\frac{\nu}{\hbar v_g} d_B\right)\right)^{-1} \tag{65}$$

For E=0 the reflection and transmission are identical to the values derived from the scattering matrix calculated by Carsten Timm et al in [15], where a delta-peak like magnetic barrier was assumed. It is also conform with the work of Nojoon Myoung [16]. The second paper considered graphen instead of HgTe-quantum wells, which due to its linear dispersion holds similar results.

The equation $T = 1 - R$ (charge conservation) used to calculate T is not a mere assumption here, as self-evident as it might seem, but can be proven by exploiting the fact, that $\sigma_z M^\dagger \sigma_z = -M$ and hence

$$\mathbb{1} = e^{M + \sigma_z M^\dagger \sigma_z} = e^M \cdot e^{\sigma_z M^\dagger \sigma_z}. \tag{66}$$

.

Proof.

$$\begin{aligned} 1-R &= \left(\langle 1| + (r^e_{\rightarrow})^* \langle 2|\right)\left(|1\rangle + r^e_{\rightarrow}|2\rangle\right) \\ &= \underbrace{\left(\left(\langle 1| + (r^e_{\rightarrow})^* \langle 2|\right) e^{\sigma_z M^\dagger \sigma_z d_B}\right)}_{=(t^e_{\rightarrow})^*\langle 1|} \underbrace{\left(e^{M d_B}\sigma_z \left(|1\rangle + r^e_{\rightarrow}|2\rangle\right)\right)}_{=t^e_{\rightarrow}|1\rangle} = T \end{aligned} \tag{67}$$

Since T and R are the same for all states, the choice of basis states used to proof the equation does not matter. □

5.1 Conductivity

The BHZ-Model as introduced above shows two edge states on each edge. This corresponds to 2 channels for charge transport on each edge, each contributing to the conductivity of the whole device with $G_0 = e^2/\hbar$, hence the total conductivity is given by

$$G_{tot} = 2G_0, \tag{68}$$

where n_c is the number of channels contributing to the charge transport. With the possibility of backscattering, as it is the case with a magnetic barrier added to the topological insulator, the conductivity will decrease though. Reflected states will not contribute to the charge transport at all, while transmitted states contribute unaltered, leading to the reflection dependent conductance of

$$G_{tot}(R) = (1-R)2G_0 \tag{69}$$

In generally the conductance would be calculated as $G = G_0 \sum_{channels}^{max} T_n$, where T_n are the Transmission values of each channel. Because T is the same for all edge states, this is reduced to equation (69) here though. Since the reflection was recently calculated the change in the conductivity device in dependency of the Energy E, the strength of the magnetic field $|B|$ and the width of the barrier d_B can be discussed and displayed.

Barrier thickness and magnetic field dependence at E=0

In the case of low energy $E \approx 0$, which in reality will be the relevant one, since the BHZ-model was designed solely for these low-energy systems, the reflection (and transmission) reduce to

$$R = \tanh^2\left(\frac{\mu_B \hat{g}|B_\parallel|}{\hbar v_g} d_B\right), \qquad T = \cosh^{-2}\left(\frac{\mu_B \hat{g}|B_\parallel|}{\hbar v_g} d_B\right) \tag{70}$$

with $B_\parallel = (B_x, B_y)^T$. Both functions are monotonous with T converging to zero ,$T \to 0$, for large magnetic fields or a great width of the barrier $\mu_B \hat{g}|B_\parallel| d_B \gg \hbar v_g$, hence R heading towards 1, as it would be expected in the first place.
At the same time, for vanishing magnetic field or barrier thickness $\mu_B \hat{g}|B_\parallel| d_B \ll \hbar v_g$ the transmission becomes 100%, which is in agreement with the results in section 5, where time reversal symmetry was not broken. The progression of the conductivity in dependence of the magnetic field and the barrier width for $E = 0$, just discussed, is displayed in figure 5.3. d_B is displayed in units of $\hbar v_g/|\hat{g}B_\parallel|$ and $|B_\parallel|$ in units of $\hbar v_g/|\hat{g}|d_B$ Measurements of the conductivity for varying $|B|$ or d_B seem promising in order to access the value of $|\hat{g}|$

Conductivity at finite Energy

Considering finite energies E two cases need to be distinguished. The first one $E < m_B \hat{g}|B_\parallel|$ is qualitatively the same as $E = 0$. For $d_B \to \infty$ the reflection R approaches 100 % and for $d_B \to 0$ the transmission T does likewise. The increased energy does cause a damping in the change of the reflection though, i.e. high energy states are more likely to pass the barrier at the same barrier

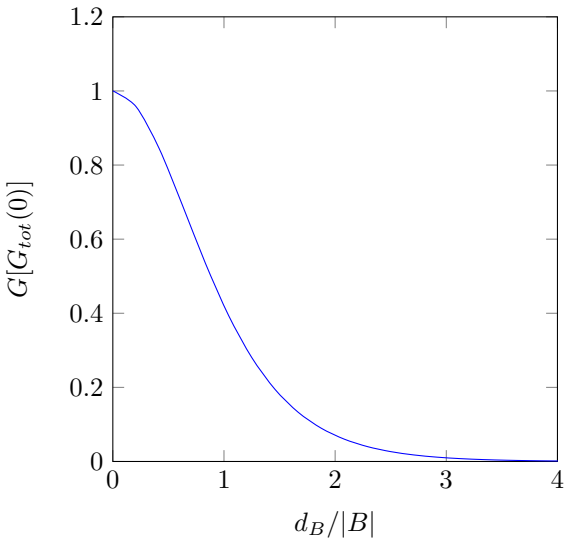

Figure 5.3: conductance G in units of $2G_0$ of a topological insulator strip with magnetic barrier d_B , respectively $|B|$.

width, as one would expect naively.
The second case $E > m_B|\hat{g}B|$ is more interesting though. In this case ν becomes an imaginary number, turning the hyperbolic functions describing R and T into trigonometric ones,($\cosh(ix) = \cos(x)$, etc.), which causes both R and T to vary periodically with d_B. More precisely R will vary between 0 and $\mu_B^2|\hat{g}B|^2/E^2$ and the periodicity will be $\pi\hbar v_g/\nu$. The dependence of the conductance on d_B for the second case is displayed in figure 5.5.

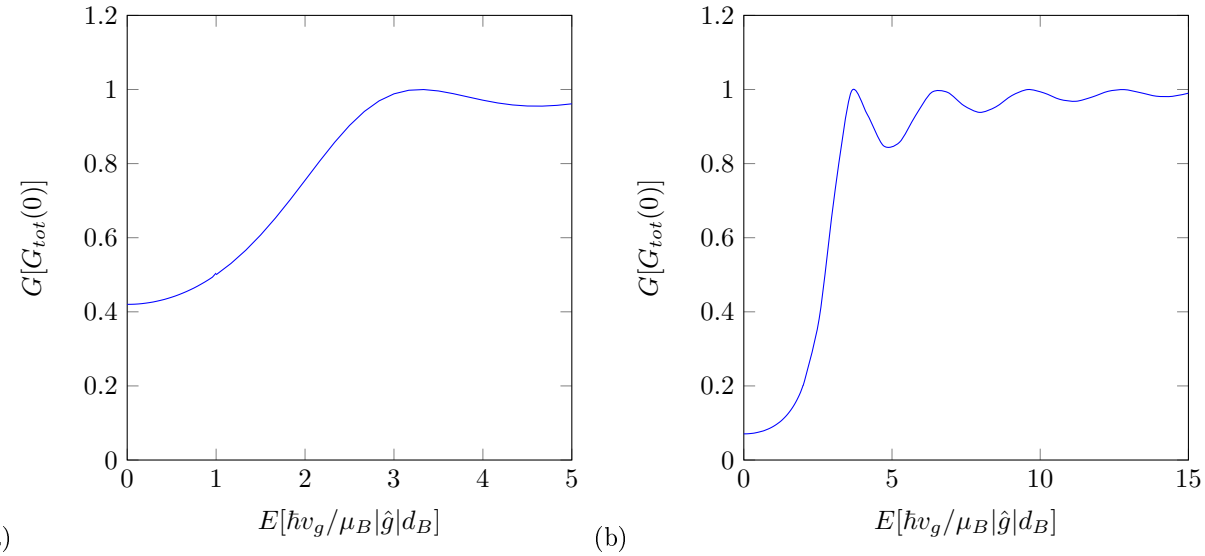

Figure 5.4: conductance G of a topological insulator strip with magnetic barrier in units of $2G_0$ in dependency of E in units of $\hbar v_g/\mu_B|\hat{g}|d_B$ for (a)$|B| = \hbar v_g/\mu_B|\hat{g}|d_B$ and (b)$|B| = 2\hbar v_g/\mu_B|\hat{g}|d_B$.)

Concerning the $|B_\parallel|$-dependence of the conductivity the limits remain unchanged independently of the energy, i.e. for $|B_\parallel| \to \infty$ R approaches 100% and for $|B_\parallel| \to 0$ R approaches 0. However, in between one has to distinguish between the two cases $\nu \in \mathbb{R}$ and $\nu \in i\mathbb{R}$ once again. In the first

case, i.e. $\mu_B\hat{g}|B_\parallel| > E$ the nonzero energy only leads to a damping in the change rate of R and T, while in the second case R is no longer monotone in $|B|$, but instead vary non periodically (ν depends on $|B_\parallel|$) between 0 and $\mu^2\hat{g}^2|B_\parallel|^2/E^2$. As a function of energy for fixed magnetic fields the reflection falls, from its value for $E = 0$, monotone till $E = \mu_B\hat{g}|B_\parallel|$ and from then on, while still converging towards 0 varies non periodically as well. Plots of the conductivity in units of $G_{tot}(0) = 2e^2/\hbar$ for both cases and depending on E with fixed $|B_\parallel|$ and depending on $|B_\parallel|$ with fixed E are displayed in figure 5.5 and figure 5.4.

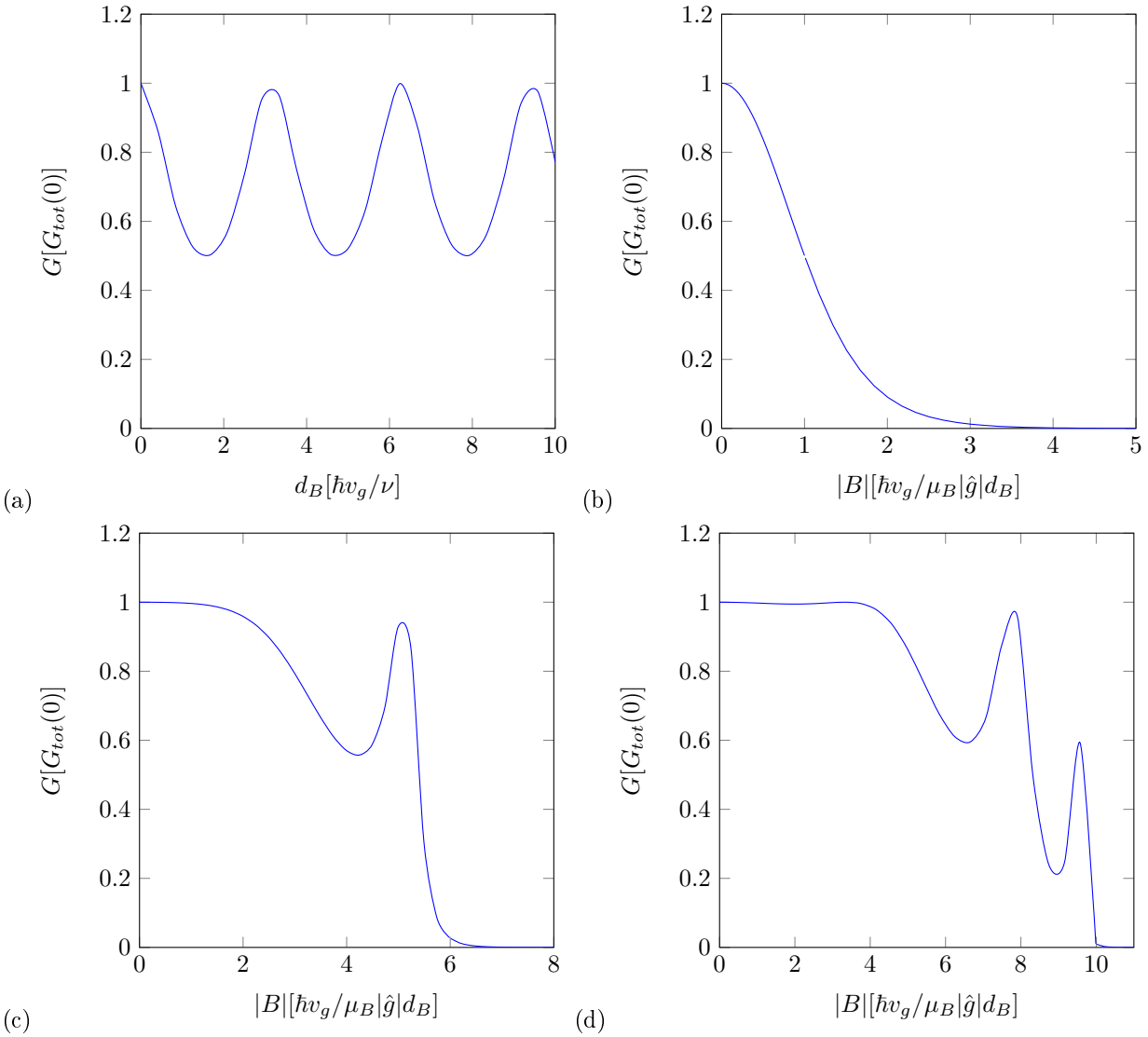

Figure 5.5: conductance G of a topological insulator strip with magnetic barrier in dependency of (a) d_B (in units of $\hbar v_g/\nu$) for $\frac{E^2}{\mu_B^2\hat{g}|B_\parallel|^2} = 2$
(b-d)in dependence of $|B_\parallel|$ (in units of $\frac{|B|\hbar v_g}{\mu_B|\hat{g}|d_B}$) for (b)$E = \frac{\hbar v_g}{\mu_B|\hat{g}|d_B}$, (c)$E = \frac{\hbar v_g}{\mu_B|\hat{g}|d_B}$ and (d)$E = 10\frac{\hbar v_g}{\mu_B|\hat{g}|d_B}$

6 Induced Superconductivity

According to BCS-theory of superconductivity, named after Bardeen, Cooper and Schrieffer, already the smallest attractive interaction between electrons in a superconductor leads to an insta-

bility of the Fermi sea and the the formation of Cooper pairs (pairs of electrons with opposite spin and momentum), which carry the supercurrent. At the same time the energy spectrum for single electrons becomes gapped:

$$E_k = \sqrt{\frac{\hbar k^2}{2m} + \Delta^2},$$

where the zero of energy and momentum is placed at the Fermi energy respectively at the Fermi momentum. [17][18]
If metals or semiconductors are placed in the direct vicinity of a superconductor Cooper pairs can tunnel into it, leading superconductivity, while the density of cooper pairs in the superconductor itself decreases. This process is called proximity effect.[19] On the other hand single electrons with energies below the superconducting gap cannot enter the superconductor. When, however an electron with an energy below the gap approaches the superconductor an electron of opposite spin and momentum can be excited, leaving behind a hole with the same spin as the original electron. The two electrons can now enter the superconductor as a cooper pair, while the hole is left behind in the metal. Of course the opposite process of a hole recombining with a cooper pair, leaving behind an electron is possible as well. This leads to a coupling between particle and hole like states.

In this section a model for HgTe/CdTe-quantum well in proximity to a superconductor will be considered. Experimentally this can be realized by putting an s-wave-superconductor on top of the quantum well in the x-y-plane. Theoretically it is accomplished by a doubling of the Hilbert space, since now apart from the original four basis states $|E\pm\rangle$ and $|H\pm\rangle$ also the corresponding hole states $|E^h\pm\rangle$ and $|H^h\pm\rangle$ have to be considered. The Hamiltonian without superconductivity of these hole states is simply a negative copy of the original BHZ-Hamiltonian. To realize the interaction between particle and hole like states coupling terms Δ_E and Δ_H are added. Δ_E couples between $|E\pm\rangle$ and $|E^h\pm\rangle$, while Δ_H does the same between $|H\pm\rangle$ and $|H^h\pm\rangle$. (It is assumed that the superconductive coupling is the same for both Kramer partners.)
This leads to the following 8×8-Hamiltonian:

$$H_S = (\epsilon + \mathcal{M}(k)s_z + Ak_x s_x\sigma_z + Ak_y s_y)\,\tau_z + (\Delta_+ + \Delta_- s_z)\,\tau_x, \tag{71}$$

where $\vec{\tau}$ are the Pauli matrices acting on the particle-hole space. (As a reminder: $\vec{s}$ are acting on the conductance band-valence band space and $\vec{\sigma}$ on the Kramer-Spin space.) A similar Hamiltonian (with additional termes to include the effects of Bulk inversion asymmetry and the linear Rashba spin orbit coupling term) was used by P.Recher et al. ([22]) to show that HgTe quantum wells with induced superconductivity can exhibit majorana edge states in presence of a Zeeman field. [23].
In the basis order $|E_1,+\rangle$; $|H_1,+\rangle$; $|E_1^h,-\rangle$; $|H_1^h,-\rangle$; $|E_1,-\rangle$; $|H_1,-\rangle$; $|E_1^h,+\rangle$; $|H_1^h,+\rangle$

$$H_S = \begin{pmatrix} H(\mathbf{k}) & \underline{\Delta} & 0 & 0 \\ \underline{\Delta} & -H(\mathbf{k}) & 0 & 0 \\ 0 & 0 & H^*(-\mathbf{k}) & \underline{\Delta} \\ & 0 & 0\underline{\Delta} & -H^*(-\mathbf{k}) \end{pmatrix} \tag{72}$$

with

$$\underline{\Delta} := \mathbb{1}_2\Delta_+ + s_z\Delta_- \tag{73}$$

and $H(\mathbf{k})$ the topmost 2×2-block of the BHZ-model, as defined in equation 11.
The edge state solutions for the first and third block are already known from earlier sections. The edge state solutions for the second and fourth, i.e. the hole-like edge states are obtained by setting

$E \to -E$ or simply $k_x \to -k_x$. The four edge states thus can be written as

$$|1,e\rangle = \begin{pmatrix} \Psi_{k_x}(x,y) \\ \vec{0} \\ \vec{0} \\ \vec{0} \end{pmatrix}; \qquad |1,h\rangle = \begin{pmatrix} \vec{0} \\ \Psi_{-k_x,}(x,y) \\ \vec{0} \\ \vec{0} \end{pmatrix}$$
$$|2,e\rangle = \begin{pmatrix} \vec{0} \\ \vec{0} \\ \Psi_{-k_x}(x,y) \\ \vec{0} \end{pmatrix}; \qquad |2,h\rangle = \begin{pmatrix} \vec{0} \\ \vec{0} \\ \vec{0} \\ \Psi_{k_x}(x,y) \end{pmatrix} \tag{74}$$

Note, that as before only one edge of the topological insulator is considered. To obtain an effective Hamiltonian for the edge states of the topological insulator in proximity of a superconductor the Hamiltonian is again projected onto these four edge states. The states $|1,e\rangle, |1,h\rangle, |2,e\rangle, |2,h\rangle$, are a basis in this reduced Hilbert space and the effective Hamiltonian in this basis is

$$H_S^{eff} = \begin{pmatrix} \hbar v_g k_x & |\alpha| e^{i\varphi_\alpha} & & \\ |\alpha| e^{-\varphi_\alpha} & -\hbar v_g k_x & & \\ & & -\hbar v_g k_x & |\alpha| e^{i\varphi_\alpha} \\ & & |\alpha| e^{-i\varphi_\alpha} & \hbar v_g k_x \end{pmatrix}, \tag{75}$$

where $\alpha(k_x) = \Delta_+ + \Delta_- \gamma(k_x)$ and $\varphi_\alpha = \arg \alpha$ were defined. It will be shown later, that the deviation of $\gamma(k_x)$ from $\gamma(0)$ is neglectable for all k_x within the bulk gap and thus from here on $\alpha(k_x)$ will be replaced by $\alpha := \alpha(0)$. The Hamiltonian is a block-diagonal matrix consisting of two Bogoliubov-de-Genne Hammiltonians $H_{BdG}(\pm k_x)$. There eigenvalues are $E = \pm\sqrt{\hbar^2 v_g^2 k_x^2 + |\alpha|^2}$, i.e. states with $E < |\alpha|$ are forbidden within the superconducting area. To find the solutions of the Schrödinger equation inside the superconducting area, we set $k_x = -i\partial_x$ and use an exponential ansatz.

$$H_{BdG} \begin{pmatrix} a_1 \\ a_2 \end{pmatrix} e^{qx} = E \begin{pmatrix} a_1 \\ a_2 \end{pmatrix} e^{qx} \tag{76}$$

Assuming $a_i \neq 0$ for one $i \in 1, 2$ leads to the secular equation

$$q = \pm \frac{\sqrt{|\alpha|^2 - E^2}}{\hbar v_g} \tag{77}$$

While this forbids the existence of edge states within the proximity of a superconductor (given their energy is in the gap) interesting physics occur, when the super conductor is placed only on one half of the topological insulator strip, say $x > 0$.[20]

6.1 Andreev-reflection

As just described now it is assumed, that a superconductor is only placed above one half of the HgTe/CdTe device, as displayed in figure 6.1, making the Hamiltonian

$$H_{NS} \begin{cases} H^{eff} & \text{for } x < 0 \\ H_S^{eff} & \text{for } x > 0 \end{cases} \tag{78}$$

While the edge states $|1\rangle$ and $|4\rangle$ approaching the superconducting regime from the left cannot enter the positive part of the x-space, as long as their energy E is smaller than α, the fact that H_S^{eff} couples electron- and hole-like states lets the possibility of Andreev reflection arise, i.e. an incoming electron is reflected as a hole and thereby creating a new cooper pair within the

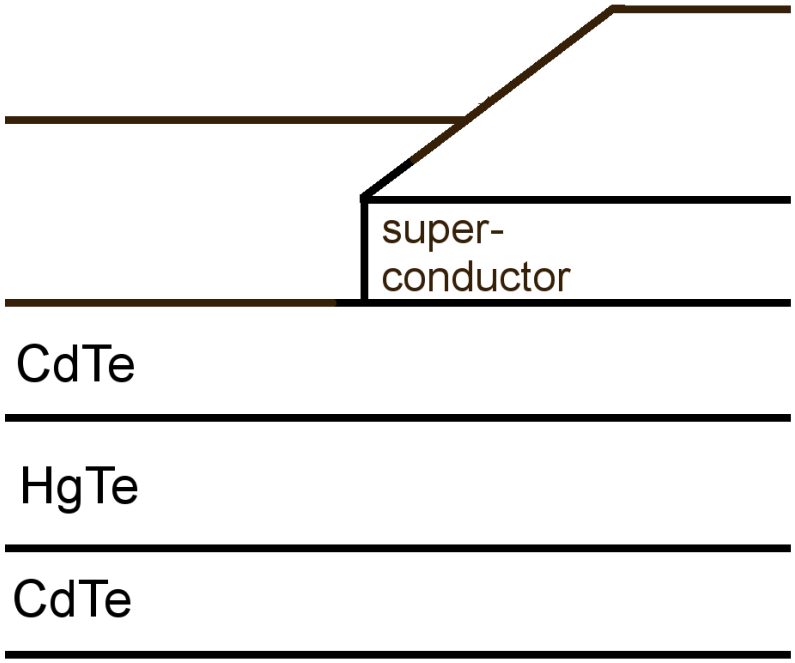

Figure 6.1: Schematic of a junction of a topological insulator and topological insulator in proximity to a superconductor-junction (NS-j)unction

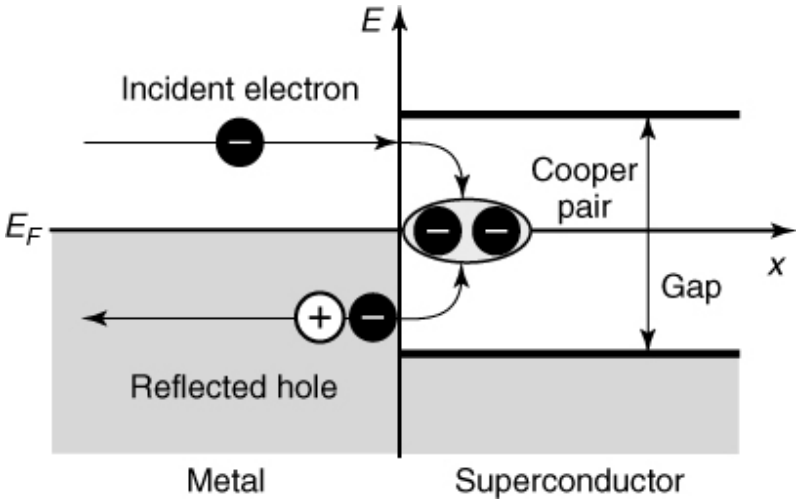

Figure 6.2: Illustration of Andreev reflection at an NS-junction as taken from [P2]

superconducting area, or an incoming hole is reflected as an electron, while absorbing a cooper pair. Compare figure 6.1.

To determine the Andreev relection amplitudes the following boundary conditions at $x = 0$ are applied to the known solutions for the Schrödinger equation.

The general solution for $x > 0$ is

$$\Phi_{x>0}(x) = (a_1|1,e\rangle + a_2|1,h\rangle + a_3|2,e\rangle + a_4|2,h\rangle)\, e^{-qx} + (b_1|1,e\rangle + b_2|1,h\rangle + b_3|2,e\rangle + b_4|2,h\rangle)\, e^{qx} \tag{79}$$

For energies $|E| < |\alpha|$ $\Phi_{x>0}(x)$ has to be an evanescent wave, so $b_i = 0$ for all i.
Then inserting the boundary condition for an incoming electron-like state

$$|1,e\rangle + r_A^e|1,h\rangle = \Phi_{x>0}^e(0) \tag{80}$$

respectively for an incoming hole state

$$|2,h\rangle + r_A^h|2,e\rangle = \Phi_{x>0}^h(0) \tag{81}$$

one sees that $\Phi_{x>0}^e(0) = |1,e\rangle + r_A^e|1,h\rangle$ and $\Phi_{x>0}^h(0) = r_A^h|2,e\rangle + |2,h\rangle$.
Reinserting both solutions into the Schrödinger equation $H_S^{eff}\Phi_{x>0}^{e/h}(x) = E\Phi_{x>0}^{e/h}(x)$ gives a system of linear equations for r_A^e respectively r_A^h with the solutions

$$r_A^e = e^{-i\varphi_\alpha}\left(\frac{E}{|\alpha|} - i\frac{\sqrt{|\alpha|^2 - E^2}}{|\alpha|}\right) = e^{i\varphi_\alpha - i\arccos\left(\frac{E}{|\alpha|}\right)} \tag{82}$$

and

$$r_A^h = e^{i\varphi_\alpha}\left(\frac{E}{|\alpha|} - i\frac{\sqrt{|\alpha|^2 - E^2}}{|\alpha|}\right) = e^{i\varphi_\alpha - i\arccos\left(\frac{E}{|\alpha|}\right)} \tag{83}$$

Note that $|r_A^{e/h}| = 1$. This means the probability of any state below the superconductor's energy gap being reflected is 100%.[20]

For energies $E > |\alpha|$ q becomes imaginary, allowing an incoming states to enter and propagate within the superconductor. Of course the same incoming state could also still create or annihilate a Cooper pair, leaving behind a counter propagating hole/electron-state. As a consequence the solutions for $x > 0$ have the following form

$$\Phi_{x>0}(x) = (a_1|1,e\rangle + a_4|2,h\rangle)\, e^{qx} + (a_2|1,h\rangle + a_3|2,e\rangle)\, e^{-qx} \tag{84}$$

With the same boundary conditions as for $|E| < |\alpha|$ for incoming electron or hole states the same solutions $\Phi_{x>0}^{e/h}(x)$ are obtained. Insertion in the Schrödinger-equation however gives the slightly different Andreev-reflection amplitudes for particles and holes with energies above the superconducting gap:

$$r_A^e = e^{-i\varphi_\alpha}\left(\frac{E}{|\alpha|} - \frac{\sqrt{E^2 - |\alpha|^2}}{|\alpha|}\right) \tag{85}$$

$$r_A^h = e^{i\varphi_\alpha}\left(\frac{E}{|\alpha|} - \frac{\sqrt{E^2 - |\alpha|}}{|\alpha|^2}\right) \tag{86}$$

It is easily seen that $|r_A| < 1$ and $|r_A| \underset{E\to\infty}{\to} 0$. [20]
Since Andreev reflection changes the sign of a state's charge as well as its propagation direction the total charge carried in one direction is doubled. Following this logic the conductivity of the topological insulator-superconductor-junctions can be written as $G(|r_A|^2) = G(0)\left(1 + |r_A|^2\right)$. In terms of energy this means, that the conductance is constant at twice its usual value, till $E = |\alpha|$ and then falls monotone converging towards $G(0)$, its value without presence of a superconductor (or magnetic barrier). The energy dependence is plotted in figure 6.3.

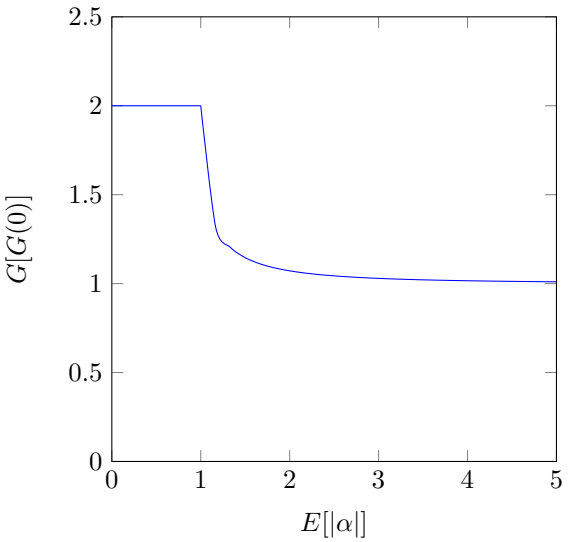

Figure 6.3: conductance G in units of $G(0)$ of NS-junction in dependency of energy in units of $|\alpha|$

6.1.1 Andreev bound states

It was seen in the previous section, that edge states (electron- and hole like alike), have a 100% chance of being Andreev reflected, at the boundary between the undisturbed topological insulator and on in vicinity of a superconductor, if their energy is below the superconductor's energy gap. This leads to the conclusion, that, if superconductors were placed on both ends of the edge, the edge states were bound in between.
In this section a set up like this is considered. Compare figure 6.4. The superconductors S_L and S_R shall be placed in the areas $x < x_L < 0$ and $0 < x_R < x$ (S-sections). The undisturbed part of the topological insulator between x_L and x_R will be referred to as N-section. The phases of the superconductors be φ_L and φ_R, not necessarily the same. The corresponding Andreev-reflection-amplitudes are $r^{e/h}_{AL/R}$. Any state with energies below $|\alpha|$ will be Andreev reflected at each border, hence limiting its motion to a finite area between x_L and x_R, yielding to discrete energies for these so called Andreev bound states.
To calculate these energy levels we define

$$\vec{a} := \begin{pmatrix} a_{L,e} \\ a_{R,e} \\ a_{L,h} \\ a_{R,h} \end{pmatrix}; \qquad \vec{b} := \begin{pmatrix} b_{L,e} \\ b_{R,e} \\ b_{L,h} \\ b_{R,h} \end{pmatrix}, \tag{87}$$

where $a_{L,e}$ is the amplitude of an elctron-like state moving from the left border to the centre of the N-section, $b_{R,h}$ is a hole-like state moving from the centre to the right border and likewise.
$\vec{a}$ and $\vec{b}$ are connected via

$$\vec{a} = \begin{pmatrix} 0 & 0 & r^h_{AL} & 0 \\ 0 & 0 & 0 & r^h_{AR} \\ r^e_{AL} & 0 & 0 & 0 \\ 0 & r^e_{AR} & 0 & 0 \end{pmatrix} \vec{b} \quad \text{and} \quad \vec{b} = \begin{pmatrix} 0 & 1 & 0 & 0 \\ 1 & 0 & 0 & 0 \\ 0 & 0 & 0 & 1 \\ 0 & 0 & 1 & 0 \end{pmatrix} \vec{a} \tag{88}$$

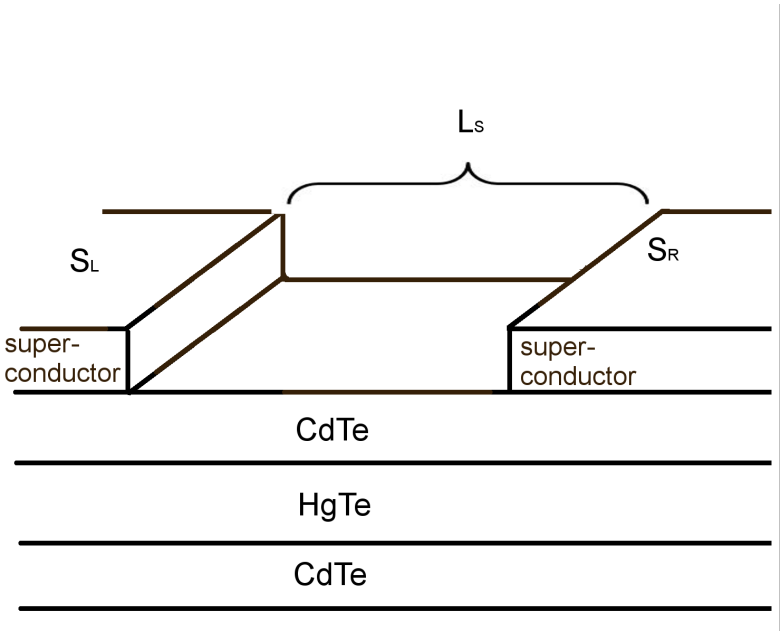

Figure 6.4: schematic of a junction consisting of a topological insulator between two topological insulators in proximity to a superconductor

Combining these two equations equation leads to

$$\underbrace{\begin{pmatrix} -1 & 0 & 0 & r^h_{AL} \\ 0 & -1 & r^h_{AR} & 0 \\ 0 & r_{AL} & -1 & 0 \\ r_{AR} & 0 & 0 & -1 \end{pmatrix}}_{:=\underline{A}} \vec{b} = 0. \tag{89}$$

Under the condition that $\vec{b} \neq 0$, this leads to

$$\begin{aligned} &\det(\underline{A}) = 0 \\ \Leftrightarrow &(1 - r^e_{AR} r^e_{AL})(1 - r^h_{AL} r^h_{AR}) = 0 \\ \Leftrightarrow &1 - e^{\pm i(\overbrace{\varphi_R - \varphi_L}^{:=\varphi})} \left(\frac{E}{|\alpha|} - i \frac{\sqrt{|\alpha|^2 - E^2}}{|\alpha|} \right)^2 \\ \Leftrightarrow &1 = \pm e^{\pm i\varphi/2} \left(\frac{E}{|\alpha|} - i \frac{\sqrt{|\alpha|^2 - E^2}}{|\alpha|} \right) \\ \Leftrightarrow &\arccos\left(\frac{E}{|\alpha|} \right) = \pm \frac{\varphi}{2} + \pi n \\ \Leftrightarrow\Leftrightarrow & \qquad\qquad E = |\alpha| \cos\left(\frac{\varphi}{2} \right) \end{aligned}$$

The relation $e^{-i \arccos(\eta)} = \eta - i\sqrt{1 - \eta^2}$ was exploited in the course of the transformations. [20] To calculate the charge transferred through this SNS-junction a little different approach is taken. Assume a small voltage V is applied to the junction. An electron/hole state thus acquires the phase $\pm k_x L_s = \pm eV L_s / v_g$, while moving from x_L to x_R, with $L_s = |x_R - x_L|$ For Andreev-bound-states to exist the total phase an electron, which is Andreev reflected at one border of the SNS-junction, i.e. turned into a hole, and then Andreev-reflected again at the other boundary, i.e.

returned to its prior state, has to be a multiple of 2π.

$$2\pi n = \pm\varphi + eV\frac{2L}{\hbar v_g} - 2\arccos\left(\frac{E}{|\alpha|}\right) \tag{90}$$

where L_s is the width of the N-part and the upper sign corresponds to a right moving electron, while the lower one corresponds to a left moving one.

Solving for E again gives

$$\arccos\left(\frac{E}{|\alpha|}\right) = \pm\frac{\varphi}{2} - n\pi + \frac{eVL_s}{\hbar v_g}, \tag{91}$$

where different values of n correspond to different branches of the arccos. Inverting it branchwise and then putting the parts together, the following result is obtained.

Keeping L as a finite size we get

$$\frac{E}{|\alpha|} = \cos\left(\frac{\varphi}{2} + \frac{eVL_s}{\hbar v_g}\right). \tag{92}$$

Note that for $V = 0$ the former result for the energy of the Andreev bound states is reproduced. Exploiting $\frac{L}{v_F}$ is the time t_L an electron or a hole need to pass from one of the the boundaries to the other one equation (92) can be rewritten as

$$\frac{E}{|\alpha|} = \cos\left(\frac{\varphi}{2} + \frac{eV}{\hbar}t_L\right). \tag{93}$$

Replacing t_L with an arbitrary time t a time dependent formula for the energy is retrieved.

$$\frac{E}{|\alpha|} = \cos\left(\frac{1}{2}\left(\varphi + \frac{eV}{\hbar}t\right)\right) := \cos\left(\frac{1}{2}\left(\varphi + \frac{\partial\varphi}{\partial t}t\right)\right). \tag{94}$$

Comparing both sides it can be see, that

$$\frac{\partial\varphi}{\partial t} = \frac{2eV}{\hbar}. \tag{95}$$

Now, looking at the time derivative of the energy allows it to calculate the current through the SNS-junction, the so called Josephson-current.[21]

$$\begin{aligned}\frac{dE}{dt} &= |\alpha|\sin\left(\frac{\varphi}{2} + \frac{eV}{\hbar}t\right)\frac{eV}{\hbar} = I\cdot V \\ \Rightarrow I(\varphi,t) &= \frac{e|\alpha|}{\hbar}\sin\left(\frac{\varphi}{2} + \frac{eV}{\hbar}t\right)\end{aligned} \tag{96}$$

There are two things to be noted. First of all unless the phase difference of the two superconductors is not a multiple of π there will be a finite current even without any voltage applied.

If on the other hand a finite voltage is applied to the junction the current is not constant but changing periodically with time. Also a higher voltage does not imply a higher current here, but merely change the periodicity.

Note that all the calculations in this section require that $|r_A^{e/h}|^2 = 1$. This can only be assumed as given for voltages not significantly changing the energy of particle- and hole-like state. In any other case the energy these states gain whenever propagating back and forth between the the boundaries would add up giving them enough energy to leave the N-section and enter one of

the S-sections.

Further note, that the calculated current results from one left or right moving electron state and the counter propagating hole it is reflected into. This means for the topological insulator device being watched the current would be 2 times higher, since there are two electron channels on each edge. Knowing this $|\alpha|$ could be measured by determining the maximum of $I(\varphi, t)$ over time. This maximum is called the critical current I_c.

Josephson current and magnetic field

Another way to manipulate the Josephson current is by applying an magnetic field through the N-section of the device. The effect of it can be calculated by replacing $k_x = \frac{p_x}{\hbar}$ by the generalized term $\hat{k_x} = \frac{p_x^{e/h} + eA_x}{\hbar}$, where $\vec{A}$ is the the vector potential.[4]

Assuming a uniform magnetic field in z-direction $\vec{A}$ can be chosen so that $A_x = B_z y$. Furthermore a magnetic field in z-direction does not influence the transmission of the N-section, since it only adds a phase to the states. This phase has opposite sign for an particle and the counter propagating hole it is reflected to, so that it can be ignored completely. The same procedure as above leads to

$$E = |\alpha| \cos\left(\frac{\varphi}{2} + \frac{eV}{\hbar}t + \frac{2\pi B_z L_s y}{\phi}\right), \tag{97}$$

where $\phi = h/2e$ is the magnetic flux quantum.

The resulting current is

$$I(\varphi, B_z, t) = \frac{e|\alpha|}{\hbar} \sin\left(\frac{\varphi}{2} + \frac{eV}{\hbar}t + \frac{2\pi B_z L_s y}{\phi}\right) \tag{98}$$

It can be seen, that the Josephson current also varies periodically with the magnetic field. Measuring the Josephson current for a smoothly varying magnetic field is a possible way to determine the critical current and thereby $|\alpha|$.

As it can be seen the current does under influence of a magnetic field not only change periodically with time but also with variation of said magnetic field. By measuring the critical current for a smoothly changed magnetic field, $|\alpha|$ can be determined.

In the experiments described in [24] and [25] this procedure has been used to show the current density along the y direction, to verify, that the charge is carried along the edges while the energy lies within the bulk gap. To understand this, the model has to be expanded a bit.

So far only the Josephson-current through the one-dimensional edge was calculated. To generalize it to 2 and 3 dimensions it is rewritten as

$$I_{1D}(\varphi, B_z, t) = I_c \sin\left(\frac{\varphi}{2} + \frac{eV}{\hbar}t + \frac{2\pi B_z L y}{\phi}\right) = I_c \Im\left(e^{i\left(\frac{\varphi}{2} + \frac{eV}{\hbar}t + \frac{2\pi B_z L y}{\phi}\right)}\right) \tag{99}$$

Interpreting a higher dimensional device as a many 1-dimensional channels in direct proximity to each other the current becomes the sum over all these channels or, by replacing the critical current by a critical current density J_c the integral over the cross section of the device. This means the current through a 2d-set-up becomes

$$I^{2D} = \Im \int_{-\infty}^{\infty} J_c(y) \exp\left[i\left(\frac{\varphi}{2} + \frac{eV}{\hbar}t + \frac{2\pi B_z L y}{\phi}\right)\right] dy. \tag{100}$$

. The Josephson current in 2- dimensional devices is the imaginary part of the Fourier-transformation of the critical current density J_c through the junction. The new critical current I_c is the maximal current, hence the absolute value of the Fourier-transformation. For our topological insulator device this means

$$I_c(B_z) = I_c^{2D} = \left| \int_{-\infty}^{\infty} J_c(y) \exp\left[i \left(\frac{2\pi B_z L y}{\phi} \right) \right] dy \right| \tag{101}$$

In reverse this gives added information about the form of the critical current density by measuring the critical current.

Exactly this method was used in the experimental papers [24] and [25] to examine the current density in a Josephson junction consisting of a HgTe quantum well with two superconductors on top of each end of the 2d-device. The measurements were taken for different chemical potentials, within and outside of the bulk energy gap, varied through different gate voltages.

How the form of the current density is obtained from these measurements shall be elaborated here at two examples.

If for example the energy of the states lies within the bulk gap of the topological insulator, hence charge should be only carried along the edges, what will be modelled by the current density $J_c^{gap} = \frac{e|\alpha|}{\hbar} (\delta(y - L/2) + \delta(y + L/2))$, the net critical current results in

$$I_c^{gap}(B_z) = \frac{2e|\alpha|}{\hbar} \cos\left(\frac{\pi B_z L_y L}{\phi} \right). \tag{102}$$

Approximating the edge states with δ-functions is of course only appropriate for wide strips, i.e. large L, nevertheless the measurements of [24] and [25] show the predicted sine-like behaviour.
For energies outside of the gap a rather uniform current density throughout junction is expected and therefore it is modelled here, very simplified again, as a rectangular function:
$J_c^{ngap}(B_Z) = J_0 \text{rect}\left(\frac{2y}{L_y}\right)$. Calculating the net critical current for this density gives a Frauenhofer-pattern:

$$I_c^{ngap}(B_z) = J_0 \frac{\sin(\pi B_z L_y L/\phi)}{\pi B_z L_y L/\phi} \tag{103}$$

Again this mirrors the experimental results from [24] and [25].

7 Combination of magnetic & superconducting barrier

Previous sections discussed the influence of magnetic barriers as well as different combinations of superconducting junctions on the conductance ot an HgTe/CdTe-quantum well. In this section though both shall be combined. The magnetic barrier be extended from $x = 0$ to $x = x_B > 0$ and the superconducting section shall range from $x = x_S x_B d$ to ∞.
The projection in the edge states of the Hamiltonian has the form

$$H_{nmns}^{eff} = \begin{cases} H^{eff} & for \;\; x < 0 \\ H_B^{eff} & for \;\; 0 < x < x_B \\ H^{eff} & for \;\; x_B < x < x_S \\ H_S^{eff} & for \;\; x_S < x \end{cases} \tag{104}$$

To calculate the conductivity G along the edge, the following vectors are defined.

$$\vec{a^*} := \begin{pmatrix} a_{e,\leftarrow} \\ a_{e,\rightarrow} \\ a_{h,\leftarrow} \\ a_{h,\rightarrow} \end{pmatrix}; \qquad \vec{b^*} := \begin{pmatrix} b_{e,\leftarrow} \\ b_{e,\rightarrow} \\ b_{h,\leftarrow} \\ b_{h,\rightarrow} \end{pmatrix}, \tag{105}$$

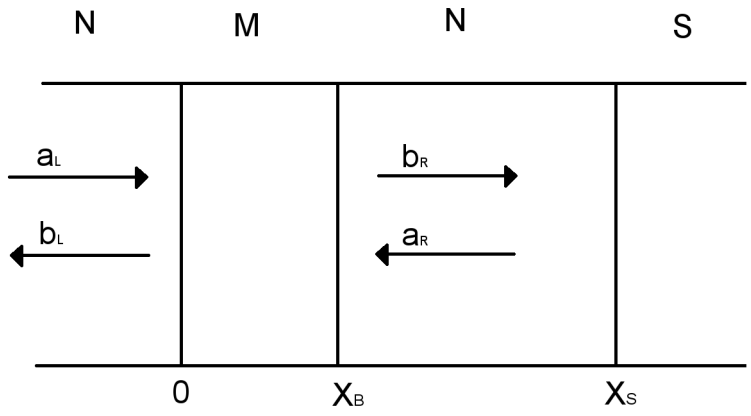

Figure 7.1: Schematic image of the NMNS-structure

where $a_{e/h,\leftrightarrow}$ is the amplitude of an electron-/hole- like state approaching the magnetic barrier from the left/right and $b_{e/h,\leftrightarrow}$ is the amplitude of an electron-/hole- like state veering away from the magnetic barrier toward the left/right.(compare figure (7.1))

The conductivity can thus be calculated as

$$G = \frac{e^2}{\hbar}\left(|a_{e,L}|^2 + |b_{h,L}|^2 - |a_{h,L}|^2 - |b_{e,L}|^2\right). \tag{106}$$

The relations between the two vectors $\vec{a}$ and $\vec{b}$ are given by

$$\vec{b^*} = \begin{pmatrix} r^e_{\leftarrow} & t^e_{\rightarrow} & & \\ t^e_{\leftarrow} & r^e_{\rightarrow} & & \\ & & r^h_{\leftarrow} & t^h_{\rightarrow} \\ & & t^h_{\leftarrow} & r^h_{\rightarrow} \end{pmatrix} \vec{a^*}; \qquad \begin{pmatrix} a_{e,\rightarrow} \\ a_{h,\rightarrow} \end{pmatrix} = \begin{pmatrix} 0 & r^h_A \\ r^e_A & 0 \end{pmatrix} \begin{pmatrix} b_{e,\rightarrow} \\ b_{h,\rightarrow} \end{pmatrix}, \tag{107}$$

where $r^{e/h}_{\leftrightarrow}$ and $t^{e/h}_{\leftrightarrow}$ are the reflection and transmission amplitudes for electron- and hole-like states approaching the magnetic barrier from the left/right and $r^{e/h}_A$ is the Andreev-reflection amplitude for electron-/hole-like states approaching the superconducting domain. Altogether these 6 equations can be written as

$$\vec{b} = \begin{pmatrix} r^e_{\leftarrow} & 0 & 0 & r^h_A t^h_{\rightarrow} \\ t^e_{\leftarrow} & 0 & 0 & r^h_A r^h_{\rightarrow} \\ 0 & r^e_A t^h_{\rightarrow} & r^e_{\leftarrow} & 0 \\ 0 & r^e_A r^h_{\rightarrow} & t^e_{\leftarrow} & 0 \end{pmatrix} \begin{pmatrix} a_{e,\leftarrow} \\ b_{e,\rightarrow} \\ a_{h,\leftarrow} \\ b_{h,\rightarrow} \end{pmatrix}. \tag{108}$$

From equation (108), it will be possible to determine $b_{e,\leftarrow}$ and $b_{h,\leftarrow}$ as functions of $a_{e,\leftarrow}$ and $a_{h,\leftarrow}$ and thus reduce the conductivity to a function of $a_{e,\leftarrow}$ and $a_{h,\leftarrow}$ as well.
Inserting

$$b_{e,\rightarrow} = t^e_{\leftarrow} a_{e,\leftarrow} + r^h_A r^h_{\rightarrow} b_{h,\rightarrow}, \tag{109}$$

into

$$b_{h,\rightarrow} = r^e_A r^e_{\rightarrow} b_{e,\rightarrow} + t^h_{\leftarrow} a_{h,\leftarrow} \underset{(109)}{=} r^e_A r^e_{\rightarrow}\left(t^e_{\leftarrow} a_{e,\leftarrow} + r^h_A r^h_{\rightarrow} b_{h,\rightarrow}\right) + t^h_{\leftarrow} a_{h,\leftarrow},$$

leads to

$$b_{h,\rightarrow} = \frac{r^e_A r^e_{\rightarrow} t^e_{\leftarrow} a_{e,\leftarrow} + t^h_{\leftarrow} a_{h,\leftarrow}}{1 - r^e_A r^h_A r^e_{\rightarrow} r^h_{\rightarrow}}, \tag{110}$$

and finally to

$$b_{e,\leftarrow}(E, a_{e,\leftarrow}, a_{h,\leftarrow}) = r_{\leftarrow} a_{e,\leftarrow} + r_A^h t_{\rightarrow} b_{h,\rightarrow} \underset{(110)}{=} r_{\leftarrow} a_{e,\leftarrow} + r_A^h t_{\leftarrow} t_{\rightarrow} \frac{r_A^e r_{\rightarrow} a_{e,\leftarrow} + a_{h,\leftarrow}}{1 - r_A^e r_A^h r_{\rightarrow}^h r_{\rightarrow}^e}. \tag{111}$$

Equation (108) is invariant under exchange of e and h and thus $b_{h,\leftarrow}(E, a_{e,\leftarrow}, a_{h,\leftarrow})$ can be obtained from $b_{e,\leftarrow}(E, a_{e,\leftarrow}, a_{h,\leftarrow})$ by interchanging e and h:

$$b_{h,\leftarrow}(E, a_{e,\leftarrow}, a_{h,\leftarrow}) = b_{e,\leftarrow}(E, a_{h,\leftarrow}, a_{e,\leftarrow}) \tag{112}$$

The conductivity can thus be calculated as

$$G(E, a_{e,\leftarrow}, a_{h,\leftarrow}) = \frac{e^2}{\hbar} \left(|a_{e,\leftarrow}|^2 + |b_{h,\leftarrow}(E, a_{e,\leftarrow}, a_{h,\leftarrow})|^2 - |a_{h,\leftarrow}|^2 - |b_{e,\leftarrow}(E, a_{e,\leftarrow}, a_{h,\leftarrow})|^2 \right) \tag{113}$$

Note that $G(E, a_{e,L}, a_{h,L}) = -G(E, a_{h,L}, a_{e,L})$, i.e. the conductivity changes sign, when the charge transport in the undisturbed topological insulator is carried out by holes instead of particles. Assuming the charge in the undisturbed regime being carried mainly by electrons, i.e. $a_{e,L} = 1$ and $a_{h,L} = 0$, $G(E, |B|) := G(E, 1, 0)$ will be referred to as the conductivity of the system. Obviously it will depend on the strength of the magnetic field $|B|$, which is already implied here. All reflection and transmission amplitudes needed for the calculation are known from previous sections and thus be simply inserted.
For example in the limit $E = 0$ the conductivity is

$$G(0, |B_\parallel|) = 1 + \underbrace{\frac{1}{\cosh^2\left(\frac{\mu_B \hat{g} |B_\parallel| x_B}{\hbar v_g}\right) + \sinh^2\left(\frac{\mu_B \hat{g} |B_\parallel| x_B}{\hbar v_g}\right)}}_{=|b_{h,\leftarrow}|^2} + \underbrace{\left(1 - \frac{1}{\cosh^2\left(\frac{\mu_B \hat{g} |B_\parallel| x_B}{\hbar v_g}\right) + \sinh^2\left(\frac{\mu_B \hat{g} |B_\parallel| x_B}{\hbar v_g}\right)}\right)^2}_{=b_{e,\leftarrow}}. \tag{114}$$

It is plotted in figure 7.2. Note that while the conductivity for $|B_\parallel| = 0$ is twice as high as the conductivity of a undisturbed topological insulator, it also decays faster with higher magnetic fields than a device with only a magnetic barrier and no superconducting regime attached to it. This can for example be seen by comparing figure 7.2 and figure 5.3.

8 Determination of Δ_E, Δ_H, g_E & g_H

Previous sections, in particular the sections 5 and 6 introduced different set ups, technically allowing it to determine the effective g-factor $\hat{g}$, transferring a coupling between the counter propagating Kramer partners in the presence of a magnetic field B, and effective superconducting order parameter α, transferring a coupling between counter propagating electron- and hole-like edge states. Both can be written in a similar way in terms of the respective subband parameters Δ_E, Δ_H, g_E and g_H. The aim of this chapter will be to survey, whether said measurements of $\hat{g}$ and α under variation of any parameters can be used to access information about Δ_E, Δ_H, g_E and g_H.

In full length the two coupling constants can written as

$$\hat{g} = \frac{1}{2}(g_E + g_H) + \gamma \frac{1}{2}(g_E - g_H) := g_+ + \gamma g_- \tag{115}$$

$$\alpha = \frac{1}{2}(\Delta_E + \Delta_H) + \gamma \frac{1}{2}(\Delta_E - \Delta_H) := \Delta_+ + \gamma \Delta_-, \tag{116}$$

where

$$\gamma = \frac{1 - w^*(\pm k_x) w(\mp k_x)}{\sqrt{(1 + |w(\pm k_x)|^2)(1 + |w(\mp k_x)|^2)}} \tag{117}$$

$$w(k_x) = \frac{A(k_x + \lambda_1)}{E + M + (B - D)(\lambda_1^2 - k_x^2)} \tag{118}$$

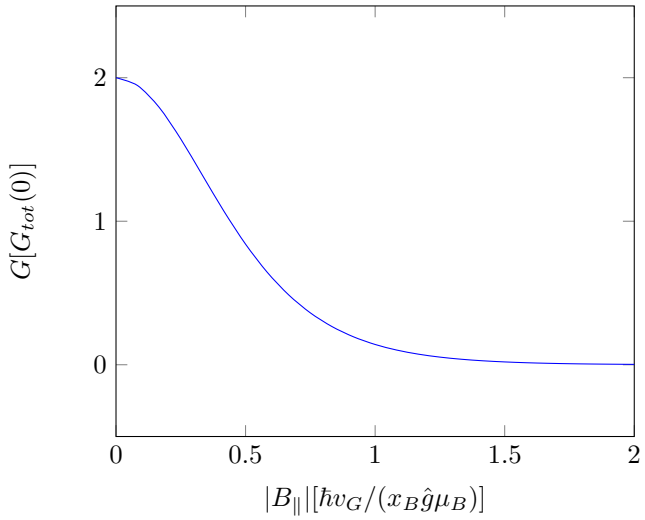

Figure 7.2: Conductivity G in units of G_0 in dependency of $|B|$ in units of $\hbar v_g/\mu_B|\hat{g}||x_B|$ for E=0

Both $|\alpha|$ and $\hat{g}$ can thus be understood as a function of γ, where $g_+ = \hat{g}(\gamma = 0)$ and and $g_- = \partial_\gamma \hat{g}$ and likewise for $\Delta_\pm$. Of course after knowing $g_\pm$ or $\Delta_\pm$ $g_{E/H}$ respectively $\Delta_{E/H}$ are easy to obtain. In other words: After measuring the two effective quantities $\hat{g}$ or α for different values of γ a linear fit would be enough to determine the subband parameters. Of course only the absolute values of $\hat{g}$ and α a accessible through measurement, however it will be shown shortly, that γ itself is a real number and therefore the two effective parameters are as well, so that this is in fact is no restriction at all.

The urging question is now, how can γ be varied to obtain measurements for different values of it. As γ depends on the edge state momentum k_x, the chemical potential C and the BHZ-parameters A, B, D and M the following sections will be devoted to separately vary their value in order to check how high their actual influence on γ is.
All variations will be carried out to first order in the particular parameter, while the remaining parameters remain constant. Since the expressions get to excessive the variations will be done for several sets of BHZ-parameters(compare 1) for each parameter around its unvaried value in the corresponding set. Since the sample parameters are rather chosen rather randomly, this procedure of course holds sure enough some uncertainty and thus rather gives an overview over the influence of the parameter than claiming to be 100% reliable for all sets of parameters.

parameter set	$d^q()$	$A_0(eV)$	$B_0(eV^2)$	$D_0(eV)$	$M_0(eV)$
1	61	3.78	-55.3	-37.8	-0.00015
2	70	3.65	-68.6	-51.2	-0.01
3	70	3.65	-70.6	-53.2	-0.001
4	n.a.	3.73	-85.7	-68.2	-0.000035
5(topologically trivial)	55	3.87	-48	-30.6	0.009

Table 2: BHZ- parameters as taken from [9],[11] and [26]

Variation of well thickness d

The parameters, which can be varied most easily are the chemical potential C and the momentum k_x. C can be varied with the application of a gate voltage and k_x by applying different voltages

to each end of the edge of the quantum well. Variation ot the two parameters however show that they have little to no influence on the values of γ, as long as the changes are small enough to keep the total energy within the bulk gap, which is necessary to maintain the existence of edge states. But comparing $\gamma\Big|_{C=k_x=0}$ for different sets of parameters leads to the assumption, that at least one of them must have a notable influence.
This means measurements of *alpha* and $\hat{g}$ with varying parameters could actually be used to deduce the values of $g_{E/H}$ and $\Delta_{E/H}$.
All of the parameters A, B, D, M depend on the geometry of the topological insulator, namely the thickness d of the quantum well, and could be calculated numerically. [11]
A variation of these parameters hence would implicitly mean a variation of d according to

$$\begin{aligned}\gamma =&\gamma\Big|_{d=d_0} + \frac{d\gamma}{dd}\Big|_{d=d_0}(\delta d) + \mathcal{O}((\delta d)^2)\\ =&\gamma\Big|_{d=d_0} + \left(\frac{\partial\gamma}{\partial w}\left(\frac{\partial w}{\partial A}\frac{\partial A}{\partial d} + \frac{\partial w}{\partial B}\frac{\partial B}{\partial d} + \frac{\partial w}{\partial D}\frac{\partial D}{\partial d} + \frac{\partial w}{\partial M}\frac{\partial M}{\partial d}\right)\delta d\right)\Big|_{d^q=d_0} + \mathcal{O}((\delta d)^2) \qquad (119)\end{aligned}$$

Since the derivatives in d are not analytically accessible the following definition is made instead.

$$\frac{\partial P_i}{\partial d^q}\delta d^q := \delta P_i = P_i - P_{i,0}, \qquad (120)$$

for $P_i \in \{A, B, D, M\}$. Inserting this in 119 leads to

$$\gamma =\gamma\Big|_{d^q=d_0^q} + \left(\frac{\partial\gamma}{\partial w}\left(\frac{\partial w}{\partial A}\Big|_{A=A_0}\delta A + \frac{\partial w}{\partial B}\Big|_{B=B_0}\delta B + \frac{\partial w}{\partial D}\Big|_{D=D_0}\delta D + \frac{\partial w}{\partial M}\Big|_{M=M_0}\delta M\right)\right) + \mathcal{O}(\delta P_i \delta P_j) \qquad (121)$$

The evaluated terms for the parameter sets from table 2 are displayed in table 3. This values

	$\gamma\big\vert_{d^q=d_0^q}$	$\frac{\partial w}{\partial A}\big\vert_{A=A_0}$	$\frac{\partial w}{\partial B}\big\vert_{B=B_0}$	$\frac{\partial w}{\partial D}\big\vert_{D=D_0}$	$\frac{\partial w}{\partial M}\big\vert_{M=M_0}$
1	-0.45	$3.9 \cdot 10^{-5}$	$-1.8 \cdot 10^{-2}$	$2.6 \cdot 10^{-2}$	0.48
2	-0.55	$1.7 \cdot 10^{-3}$	$1.7 \cdot 10^{-2}$	$2.3 \cdot 10^{-2}$	0.31
3	-0.56	$2.4 \cdot 10^{-4}$	$1.7 \cdot 10^{-2}$	$2.2 \cdot 10^{-2}$	0.43
4	-0.63	$7.1 \cdot 10^{-6}$	$-1.5 \cdot 10^{-2}$	$1.9 \cdot 10^{-2}$	0.38

Table 3: Variation in various parameters for parameter sets 1-3

give at least a little insight on the influence the various parameters have on γ. δA for example would have to be of magnitude 10^2 to 10^4 to change γ significantly. Comparing values of A at different well-thickness (table 2) this is surely not to expect and therefore deviation caused by A are assumably neglectable.
In terms of B and D things look differently. Changes in B and D of magnitude 10^1 already have measurable influence on γ. Variations of this size can be obtained by tuning the well thickness by several , as seen in table 2.
Concerning the mass term M even variation of $10^{-1}eV$ would be noticeable. Looking at table 2 with this in mind, mass-changes of this magnitude seem possible.

Conclusion

As mentioned before only changes in B, D and M seem to have measurable influence on γ, while variations of A, C and k_x very little to no influence, as long as $\hat{g}$ and α are measured via transport properties of the edge channels, as suggested in previous sections.

The influential parameter B, D and M all depend on the thickness d of the quantum well(,as well as A). Hence obtaining values of $\hat{g}$ and α for different values of γ would require the growth of various HgTe/CdTe-quantum wells of different thickness d. Since the suggested transport experiments to determine the coupling constants require edge states, and these only exist in the inverted regime $d > d_c \approx 6.3nm$ is required, while d still has to be small enough to maintain the 2-dimensional character of the system.

Concerning the actual measurement of the coupling constants the measurement of the Josephson current through a SNS-junction seems to be most promising to determine α, while $\hat{g}$ is probably achieved easiest from the decay of conductivity for a smoothly increasing magnetic barrier.

List of Figures

List of Tables

References

[1] "Supersymmetry in heterojunctions: band-inverting contact on the basis of Pb1-xSnxTe and Hg1-xCdxTe", Pankratov, Pakhomov, Solid state communications 61 (2):93-96

[2] "Quantum Spin Hall insulators state in HgTe Quantum Wells", König, Wiedman, Brüne, Roth, Buhmann, MOlenkamp, Qi, Zhang; Science 318(5851):766-770

[3] "Festkörperphysik Einführung in die Grundlagen", Ibach Lüth, 7. Aufglage, Springer

[4] "Grundkurs theoretische Physik 5/2 Quantenmachanik - Methoden und Anwendungen", Nolting, 7. Auflage, Springer

[5] "Colloquium: topological insulators", M.Z. Hasan, C.L. Kane,REVIEWS OF MODERN PHYSICS, VOLUME 82, OCTOBER–DECEMBER 2010

[6] "Primer on topological insulators", A. Altland, L. Fritz

[7] "Topological insulators and topological superconductors", B. A. Bernevig, T.L. Hughes, Princeton University Press, 2013

[8] $https://en.wikipedia.org/wiki/Chern_class$, 16.7.15

[9] "Topological insulators and superconductors", Xiao-Liang Qi, Shou-Cheng Zhang ,arXiv:1008.2026 [cond-mat.mes-hall] 12 Aug 2010

[10] "Quantum Spin Hall Effect and Topological Phase Transition in HgTe Quantum Wells" B. Andrei Bernevig,Taylor L. Hughes,Shou-Cheng Zhang, Science 314, 1757(2006)

[11] "Fingerprint of different spin–orbit terms for spin transport in HgTe quantum wells" D. G. Rothe, R W Reinthaler1, C-X Liu1 L. W. Molenkamp, S-C Zhang and E. M. Hankiewicz,New Journal of Physics 12 (2010) 065012 (22pp),doi:10.1088/1367-2630/12/6/065012

[12] $https://de.wikipedia.org/wiki/Kramers-Theorem$, 20.07.15

[13] "Helical edge states in multiple topological mass domains", P.Michetti, P.H.Penteado,J-C.Euges,P.Recher, arXiv:1209.2313v3 [cond-mat.mes-hall], 22 Nov 2012

[14] "Finite size effects on helical edge states in a Quantum Spin-Hall System", Bin Zhou, Hai-Zhou Lu Rui-Lin Chu, Schun-Quing Shen, and Qian Niu, PRL 101,246807(2008)

[15] "Transport through a quantum spin Hall quantum dot", Carsten Timm, PHYSICAL REVIEW B 86, 155456 (2012)

[16] "Tunneling of Dirac fermions through a magnetic barriers in graphene", Nojoom Myoung, Physikca E 4 (2009) 70-72

[17] "Introduction to superconductivity", Michael Tinkham, McGraw-Hill Inc, sevond edition

[18] "Superconductivity of Metals and Alloys",P.G. De Gennes, Advanced book classics

[19] $https://de.wikipedia.org/wiki/Proximity-Effekt\_\%28Supraleitung\%29$,30.07.15

[20] "Quantum transport- introduction to Nanoscience" Yuli V. Nazarow, Yaroslav M. Blanter, Cambridge university press

[21] "Possible new effects in superconductive tunneling " B.D.Josephson Cacendish labratory, Cambridge England, Physics Letters Vol.1 Nr.7, 01.07.1952

[22] "Chiral Majorana edge states in HgTe quantum wells", L. Weiterhofer , P. Recher, New Journal of Physics 15 (2013) 085008 (19pp)

[23] "Andreev spectroscopy of doped HgTe quantum wells", M. Guigou and J. Cayssol, PHYSICAL REVIEW B82, 115312(2010)

[24] "Edge-mode Superconductivity in a Two Dimensional Topological Insulator", Vlad S. Pribiag, Arjan J.A. Beukman,1, Fanming Qu,1, Maja C. Cassidy, Christophe Charpentier, Werner Wegscheider, and Leo P. Kouwenhoven,
arXiv:1408.1701v1 [cond-mat.mes-hall] 7 Aug 2014

[25] "Induced superconductivity in the quantum spin Hall edge" Sean Hart, Hechen Ren, TimoWagner, Philipp Leubner, Mathias Mühlbauer, Christoph Brüne, Hartmut Buhmann, LaurensW. Molenkamp and Amir Yacoby, Natur physics, 3 Aug 2014,
DOI: 10.1038/NPHYS3036

[26] "Single valley Dirac fermions in zero-gap HgTe quantum wells" B. Büttner, C.X. Liu, G. Tkachov, E.G. Novik, C. Brüne, H. Buhmann, E.M. Hankiewicz, P. Recher, B. Trauzettel, S.C. Zhang and L.W. Molenkamp http://arxiv.org/abs/1009.2248v2

[P1] lecture notes from Shoucheng Zhang, Stanford University, Hongkong 2010, *http* : *//www.physics.hku.hk/ ctcp/HKForum*10/*talks/Zhang* − *SC* − *HKFP*2010.*pdf*

[P2] "What is what in the Nanoword", Victor E. Borisenko, Stefano Ossicini, *http* : *//wiley* − *vch.e* − *bookshelf.de/products/reading* − *epub/product* − *id*/792675/*title/What*%2*Bis*%2*BWhat*%2*Bin*%2*Bthe*%2*BNanoworld.html*?*lang* = *en*